Computation and Analysis of Natural Compliance in Fixturing and Grasping Arrangements

Qiao Lin, Joel W. Burdick, and Elon Rimon

***Abstract*—This paper computes and analyzes the natural compliance of fixturing and grasping arrangements. Traditionally, linear-spring contact models have been used to determine the natural compliance of multiple contact arrangements. However, these models are not supported by experiments or elasticity theory. We derive a closed-form formula for the stiffness matrix of multiple contact arrangements that admits a variety of nonlinear contact models, including the well-justified Hertz model. The stiffness matrix formula depends on the geometrical and material properties of the contacting bodies and on the initial loading at the contacts. We use the formula to analyze the relative influence of first- and second-order geometrical effects on the stability of multiple contact arrangements. Second-order effects, i.e., curvature effects, are often practically beneficial and sometimes lead to significant grasp stabilization. However, in some contact arrangements, curvature has a dominant destabilizing influence. Such contact arrangements are deemed stable under an all-rigid body model but, in fact, are unstable when the natural compliance of the contacting bodies is taken into account. We also consider the combined influence of curvature and contact preloading on stability. Contrary to conventional wisdom, under certain curvature conditions, higher preloading can increase rather than decrease grasp stability. Finally, we use the stiffness matrix formula to investigate the impact of different choices of contact model on the assessment of the stability of multiple contact arrangements. While the linear-spring model and the more realistic Hertz model usually lead to the same stability conclusions, in some cases, the two models lead to different stability results.**

***Index Terms*—Compliance, contact models, curvature effects, fixture planning, fixturing, grasp planning, grasping, stability, stiffness, stiffness matrix.**

I. Introduction

THIS PAPER is concerned with multiple contact arrangements where the chief source of compliance is the natural compliance of the contacting bodies, i.e., compliance that arises from material deformation in the vicinity of the contacts. In grasping applications, the contacting bodies are usually treated as ideal rigid bodies. Compliance typically appears in these applications as a design parameter which is implemented by various stiffness-control methods [1], [7], [12], [25], [26], [34]. The stiffness-control approach is fully justified in multifinger grasps where compliance introduced at the finger joints dominates the natural compliance at the fingertips. However, in many grasping applications, the natural compliance of the contacting bodies plays an important role. Consider, for example, fixturing for manufacturing or assembly [5], [23], [33]. In these applications, a workpiece is fixtured with some *preloading* forces by several fixturing elements (or *fixels*). The workpiece need not only be stable against external perturbations, but it must also stay within a specified tolerance in response to machining or assembly forces [3], [18], [22]. Another example is multifinger grasps with soft fingertips, where the natural compliance of the fingertips plays a dominant role in the overall grasp compliance [36]. This paper is concerned with the computation and analysis of the natural compliance of multiple contact arrangements based on realistic contact models.

The stiffness matrix is a key analytical tool for characterizing the compliance of a given contact arrangement. It predicts the qualitative stability of the contact arrangement, as well as the quantitative deflection of the workpiece in response to an applied external wrench (i.e., force and torque). With the exception of the work by Howard and Kumar [19] discussed below, traditionally, linear-spring contact models have been used by robotics researchers. For example, Nguyen [25] and Funahashi *et al.* [14] investigate the stability of compliant grasps where the fingers are modeled as linear springs. Xiong *et al.* analyze the dynamic stability of compliant grasps using a linear spring-damper model for the fingers [35]. Using linear-spring models, Donoghue *et al.* [11] and Ponce [27] investigate stable two-dimensional (2-D) and three-dimensional (3-D) workpiece fixturing. However, the use of linear springs to model natural compliance associated with material deformation is generally *not* supported by experimental or theoretical results, and can lead to significant analysis errors. For example, consider the fixtured workpiece shown in Fig. 1, which is subjected to an external torque. In Section VI, we compare the part's deflection calculated with compliance modeled by the linear spring and nonlinear Hertz contact models, respectively. The calculated deflection would bound the tolerances of any machining or assembly operation that uses this fixturing arrangement. Our calculations show that the two contact models can predict *significantly different deflections*, and hence, the linear model may not faithfully predict the deflections that are likely to be encountered in physical fixturing arrangements. Furthermore, it is not always clear how to determine the stiffness coefficients of the linear springs

Manuscript received January 23, 2002; revised January 29, 2003. This paper was recommended by Associate Editor Z. Li and Editor I. Walker upon evaluation of the reviewers' comments. This work was supported in part by Grant IIS-9901056 (Experiments, Modeling, and Automatic Planning for Fixturing and Gripping), in part by Grant IRI-9503835 (Robotic Motion Planning with Quasi-Static Force Constraints), and in part by Grant NSF9402726 [NSF Engineering Research Center for Neuromorphic Systems Engineering (CNSE)].

Q. Lin is with the Department of Mechanical Engineering, Carnegie Mellon University, Pittsburgh, PA 15213 USA (e-mail: qlin@andrew.cmu.edu).

J. W. Burdick is with the Department of Mechanical Engineering, California Institute of Technology, Pasadena, CA 91125 USA (e-mail: jwb@robotics.caltech.edu).

E. Rimon is with the Department of Mechanical Engineering, Technion, Israel Institute of Technology, Haifa 32000, Israel.

Digital Object Identifier 10.1109/TRO.2004.829470

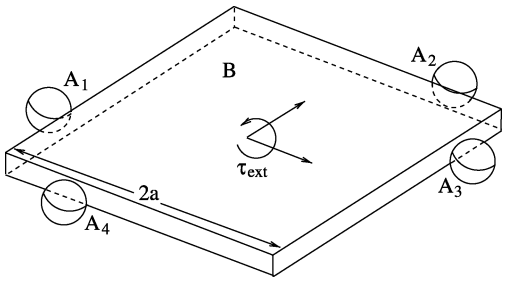

Fig. 1. Workpiece fixtured by four fixels is subjected to an external torque (the supporting plane is not shown).

from first principles. These shortcomings of the linear-spring model prevent automated planning algorithms from accurately computing fixturing arrangements, fixture reaction forces, and fixtured object deflections from computer-aided design (CAD) models.

We describe in this paper a general class of nonlinear compliant contact models using overlap functions and apply this formulation to compute and analyze the stiffness matrix of multiple contact arrangements. The resulting stiffness matrix admits a general class of compliant contact models that includes the experimentally verified and theoretically justified Hertz contact model [17] (reviewed below). The formula also admits the nonlinear contact model proposed by Kao [36] for soft fingertips. When applied to the linear-spring model, the formula agrees with the results of [11], [25], and [27]. When applied to the Hertz model, the stiffness matrix offers a realistic description of grasp compliance for many situations of practical interest. Since the Hertzian stiffness matrix can be computed from first principles, its parameters can be automatically determined from the material and geometrical properties of the contacting bodies. It is, therefore, suitable for automated fixture analysis and synthesis.

Howard and Kumar [19] present an earlier derivation of the stiffness matrix using a different approach. They first linearize the Hertz compliance relationship at the contacts and then compute the stiffness matrix associated with the linearized contacts. In contrast, we derive the formula using a configuration-space approach. First, we express the grasp's total elastic energy as a function of the object's configuration. Then we obtain the grasp stiffness matrix by computing the second derivative of the elastic energy directly in the object's configuration space. Moreover, Howard and Kumar neglect the effect of local deformation at the contacts on the curvature of the contacting bodies, while we provide the exact stiffness formula which includes this effect. The derivation of the stiffness matrix formula in the object's configuration space is only one contribution of this paper. Our stiffness matrix formula carries the choice of contact model as a parameter; it explicitly shows the terms associated with first- and second-order geometrical effects, as well as terms associated with the preloading forces. We use these features to obtain fundamental results on the dependency of grasp stability on various geometrical effects, on the preloading forces, and on the choice of contact model. These results are described in the following paragraph.

After introducing basic assumptions in the next section, we describe in Section III the modeling of compliant contacts with overlap functions. The Hertz model is then reviewed in the context of overlap functions. In Section IV, we derive the stiffness matrix formula using overlap functions. The formula is then subjected to several important analyses that have not appeared in the literature before. First, in Section V, we analyze the combined effect of first- and second-order geometrical effects on grasp stability. We show that destabilizing curvature effects are typically negligible relative to stabilizing first-order effects, while *stabilizing curvature effects can generate forces comparable with those generated by first-order geometrical effects*. This possibility provides physical basis for curvature-based reduction in the number of contacts in grasping and fixturing [4], [9], [10], [28], [29]. On the other hand, curvature effects can destabilize certain grasps deemed stable by first-order effects. This possibility implies that *certain grasps which are stable under the ideal rigid-body model are unstable when the natural compliance of the contacting bodies is taken into account*. In Section VI, we clarify the combined influence of curvature and preloading on grasp stability. According to conventional wisdom, increased preloading leads to greater grasp instability [8], [24]. We show that, depending on the curvature at the contacts, *increased preloading can either stabilize or destabilize a grasp*. In Section VII, we study the influence of different choices of contact model on the determination of grasp stability. While the linear-spring model and the Hertz model usually lead to the same stability conclusions, *in some special cases, linear-spring models can lead to erroneous prediction of stability*. Finally, the concluding section summarizes the results and discusses limitations of our approach.

II. Basic Assumptions and Terminology

A grasping or fixturing arrangement consists of an object $\mathcal{B}$ held by bodies $\mathcal{A}_1, \ldots, \mathcal{A}_k$ corresponding to fingertips or fixels. In the following, we use the language of grasping and call the contacting bodies "fingers." We make the following two assumptions. First, we assume that each finger touches $\mathcal{B}$ through a *frictionless* point contact, such that the boundaries of the bodies are smooth in the vicinity of the contacts. The frictionless contact assumption allows us to analyze the influence of first- and second-order geometrical effects, as well as preloading, on grasp compliance, without the additional complexity associated with friction effects. The inclusion of friction in the compliance analysis is sketched in Section VIII. It will be shown that under certain assumptions, friction only enhances the stability of frictionless grasps. Moreover, prediction of object deflection due to external load under a frictionless contact model provides a conservative upper bound on the deflection generated in the presence of friction. Since friction usually depends on varying environmental conditions such as temperature and humidity [5], it is reasonable to consider the limiting case of frictionless grasps.

Our second key assumption is that the bodies are *quasi-rigid*, so that deformations due to compliance effects are localized to the vicinity of the contacts. This assumption holds with reasonable accuracy for bodies which do not possess slender substructures. We focus on grasps where the fingers are *stationary*. Since the fingers are stationary and only $\mathcal{B}$ can move, we may study the grasp in $\mathcal{B}$'s *configuration space* (c-space). Moreover, the

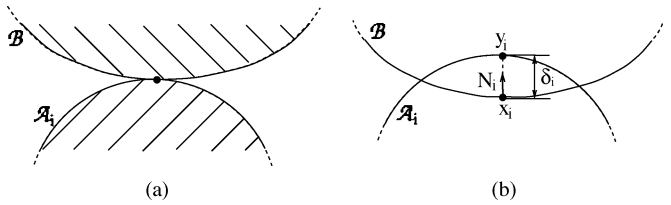

Fig. 2. (a) An initial point contact. (b) After a relative approach of δ_i.

quasi-rigidness assumption allows us to describe the overall motion of $\mathcal{B}$ relative to the fingers using rigid-body kinematics.

The c-space of $\mathcal{B}$ is a 6-D manifold $\mathcal{C}$ whose coordinates correspond to the position and orientation of $\mathcal{B}$. Given a fixed frame $\mathcal{F}_W$ and a frame $\mathcal{F}_B$ attached to $\mathcal{B}$, the configuration of $\mathcal{B}$ is specified by the position $d \in \mathbb{R}^3$ and orientation $R \in SO(3)$ of $\mathcal{F}_B$ relative to $\mathcal{F}_W$, where $SO(3)$ is parametrized by $\theta \in \mathbb{R}^3$ (e.g., using exponential coordinates). From now on, we do not distinguish between the c-space manifold $\mathcal{C}$ and its coordinate parametrization by $q = (d, \theta) \in \mathbb{R}^3 \times \mathbb{R}^3$. The *tangent space* to $\mathcal{C}$ at q, denoted $T_q\mathcal{C}$, is the set of all velocities of $\mathcal{B}$ at q. Tangent vectors take the form $\dot{q} = (v, \omega)$, where $v \in \mathbb{R}^3$ and $\omega \in \mathbb{R}^3$ are the linear and angular velocities of $\mathcal{B}$, as viewed in $\mathcal{F}_W$. Similarly, the *wrench space* at q, denoted $T_q^*\mathcal{C}$, is the set of all wrenches acting on $\mathcal{B}$ at q. A wrench takes the form $\boldsymbol{w} = (f, \tau)$, where $f \in \mathbb{R}^3$ and $\tau \in \mathbb{R}^3$ are the force and torque acting on $\mathcal{B}$, as viewed in $\mathcal{F}_W$. When the object and fingers are planar bodies, the z axis of the world and body frames is chosen perpendicular to the plane.

Next we review the condition for an equilibrium grasp. Let x_i be the contact point of the ith finger with $\mathcal{B}$, and let N_i be the inward-pointing unit normal to $\mathcal{B}$ at x_i [see Fig. 2(b)]. Let $\boldsymbol{F}_i$ be the force acting on $\mathcal{B}$ at x_i. The wrench generated by $\boldsymbol{F}_i$ is $\boldsymbol{w}_i = (\boldsymbol{F}_i, (Rz_i) \times \boldsymbol{F}_i)$, where z_i is the contact point expressed in $\mathcal{F}_B$, and R is the orientation matrix of $\mathcal{B}$. By definition, a k-finger arrangement is an *equilibrium grasp* if, in the absence of any external wrench, the net wrench on $\mathcal{B}$ is zero, shown as follows:

$$\boldsymbol{w}_1 + \cdots + \boldsymbol{w}_k = \vec{0}. \tag{1}$$

In our frictionless case, the contact forces act along the surface normals, so that $\boldsymbol{F}_i = F_i N_i$ where F_i is the magnitude of the ith force. In this case, the wrenches are given by $\boldsymbol{w}_i = F_i(N_i, (Rz_i) \times N_i)$ for $i = 1, \ldots, k$.

III. Modeling Contact Compliance

This section reviews a general approach for modeling the compliant contact of quasi-rigid bodies, using the notion of overlap [31]. The classical Hertz contact theory is then reviewed and shown to be a special case of the overlap approach.

A. Overlap Representation

Let $\mathcal{B}$ be in point contact with a stationary finger $\mathcal{A}_i$. When $\mathcal{B}$ is displaced toward $\mathcal{A}_i$, the surfaces of the two bodies deform in the vicinity of the contact. We wish to ignore the details of surface deformation and model the resultant contact force in a lumped parameter way as a function of the displacement of $\mathcal{B}$. Such a model can be based on *overlap functions* as follows.

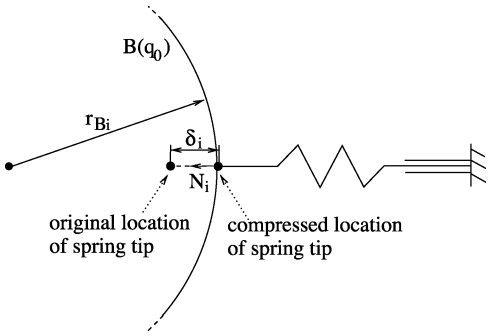

Fig. 3. Linear-spring model.

Let $\mathcal{B}(q)$ denote the subset of $\mathbb{R}^3$ occupied by the undeformed shape of $\mathcal{B}$, where $\mathcal{B}$ is at a configuration q. Let $\partial\mathcal{B}(q)$ denote the boundary of $\mathcal{B}(q)$, and let $\partial\mathcal{A}_i$ denote the boundary of the undeformed finger $\mathcal{A}_i$. Rather than solve for the surface deformations due to compliant contact, conceptually imagine that the rigid shape of $\mathcal{B}$ could freely penetrate the rigid shape of $\mathcal{A}_i$ when $\mathcal{B}$ approaches $\mathcal{A}_i$. The *overlap* between $\mathcal{B}(q)$ and $\mathcal{A}_i$, denoted $\delta_i(q)$, is the minimum amount of translation that would separate the undeformed shape of $\mathcal{B}$ from that of $\mathcal{A}_i$. At the initial contact configuration, $\mathcal{B}(q)$ and $\mathcal{A}_i$ intersect at a point, and $\delta_i(q) = 0$. Similarly, $\delta_i(q)$ is zero when $\mathcal{B}(q)$ is disjoint from $\mathcal{A}_i$. When $\mathcal{B}(q)$ overlaps $\mathcal{A}_i$, there exists a unique *overlap segment*[1] with endpoints $x_i \in \partial\mathcal{B}(q)$ and $y_i \in \partial\mathcal{A}_i$, such that $\delta_i = \|x_i - y_i\|$ (see Fig. 2). Moreover, the normals to $\partial\mathcal{B}(q)$ and $\partial\mathcal{A}_i$ at x_i and y_i are collinear with the overlap segment. The overlap $\delta_i(q)$ is generally a nonlinear function of q, and is a smooth function of q at configurations where $\delta_i(q)$ is a small positive number.

The overlap δ_i is known in the contact mechanics literature as the *relative approach* of the two bodies [15], [20]. Also in agreement with the contact mechanics literature, the contact force is assumed to act along the overlap segment $\overline{x_i y_i}$. The force's magnitude, denoted F_i, is assumed to depend on the overlap in terms of a function f_i, as follows:

$$F_i = f_i(\delta_i). \tag{2}$$

We refer to f_i as the *stiffness function* at the ith contact. The function f_i is required to be differentiable, zero when its argument is zero, and monotonically increasing in its argument δ_i. In particular, $f_i(\delta_i)$ and its derivative $f_i'(\delta_i)$ are positive when δ_i is positive. To summarize, the contact force has magnitude $F_i = f_i(\delta_i)$ and direction N_i, where N_i is the inward pointing unit normal to $\mathcal{B}$ at the endpoint x_i of the overlap segment (Fig. 2).

Example 1 (Linear-Spring Example): To provide continuity with the existing literature [16], [25], [27], consider an object held by linear springs (Fig. 3). Each spring is assumed to act along a *fixed* direction aligned with $\mathcal{B}$'s surface normal at the contact. At an equilibrium configuration q_0, the overlap $\delta_i(q_0)$ is the net compression of the ith spring, and the contact-force magnitude is $F_i = \kappa_i \delta_i(q_0)$, where κ_i is the spring stiffness. Thus, in this case, the stiffness function f_i is linear in δ_i (note that

[1]The overlap segment is unique for all sufficiently small overlaps δ_i [31].

$\delta_i(q)$ is still generally nonlinear in q). However, this paper focuses on modeling the natural compliance of contacting bodies, for which the Hertz contact model is more suitable.

B. Hertz Contact Model

The Hertz contact model (1882) describes the interaction between two quasi-rigid bodies [17], [20], and this model has been extensively verified by experiments (see, e.g., [13]). We summarize the Hertz model and place it in our framework by showing that it corresponds to a particular choice of a stiffness function f_i. Hertz theory considers two quasi-rigid bodies, $\mathcal{B}$ and $\mathcal{A}_i$, that initially touch at a single point. When $\mathcal{B}$ presses against $\mathcal{A}_i$, the deformed bodies touch over a finite contact area, while the undeformed shapes of $\mathcal{B}$ and $\mathcal{A}_i$ are considered to have an overlap δ_i. The forces acting over the contact area are specified by a *contact pressure* expression, whose integral gives the net contact force of magnitude F_i.

The Hertzian formula for F_i depends on the curvature of the contacting bodies. Let $\mathcal{S}$ be a surface, and let $N(x)$ denote the unit normal to $\mathcal{S}$ at a point x on $\mathcal{S}$. The derivative of $N(x)$ along the surface $DN(x)$ is the *curvature matrix* (or Weingarten map [32]) of the surface. Let the curvature matrices of $\mathcal{B}$ and $\mathcal{A}_i$ at the initial contact point be L_{B_i} and L_{A_i}. The reciprocals of the curvature matrix eigenvalues are the *principal radii of curvature* (or simply radii of curvature) of the surface. The negative, zero, or positive sign of the radii of curvature signifies that the surface is concave, flat, or convex in the direction corresponding to the radius of curvature. The *relative curvature matrix* of $\mathcal{B}$ and $\mathcal{A}_i$ at the initial contact point is defined by $L_{\rm rel} = L_{A_i} + L_{B_i}$. The reciprocals of the eigenvalues of $L_{\rm rel}$, denoted $r^1_{\rm rel}$ and $r^2_{\rm rel}$, are the *principal radii of relative curvature* (or simply the radii of relative curvature). The matrix $L_{\rm rel}$ is positive definite in the generic case, where the second-order approximations to the undeformed bodies are in point contact.

In the Hertz model, the contact area is a planar ellipse centered at the original contact point, with principal semiaxes a and b $(a \geqslant b)$. For a quasi-rigid contact, a and b are small when compared with the radii of curvature at the contacts. The eccentricity of the contact ellipse b/a depends only on the relative curvature of the undeformed bodies. The ratio b/a is given in terms of an eccentricity parameter $e = (1 - b^2/a^2)^{1/2}$, as follows:

$$\frac{(1-e^2)^{-1}\mathbf{E}(e) - \mathbf{K}(e)}{\mathbf{K}(e) - \mathbf{E}(e)} = \frac{r^1_{\rm rel}}{r^2_{\rm rel}} \tag{3}$$

where $\mathbf{K}(e)$ and $\mathbf{E}(e)$ are complete elliptic integrals. The parameter e appears in the following key equation for the magnitude F_i of the contact force:

$$F_i = \frac{4}{3}\beta(e)E^* r_e^{\frac{1}{2}} \delta_i^{\frac{3}{2}} \tag{4}$$

where $r_e = (r^1_{\rm rel} r^2_{\rm rel})^{1/2}$. In this formula, $\beta(e)$ is an expression which depends on e and is listed below, and E^* is determined from material properties as follows: $(E^*)^{-1} = (1-\nu^2_{A_i})/E_{A_i} + (1-\nu^2_{B_i})/E_{B_i}$, where E_{A_i} and E_{B_i} are Young's moduli, and ν_{A_i} and ν_{B_i} are Poisson's ratios of $\mathcal{A}_i$ and $\mathcal{B}$ at the ith contact. Note that (4) is an expression of the form $F_i = c_i \delta_i^{3/2}$, which implies that the Hertz contact model corresponds to a particular choice of the stiffness function f_i in the overlap model. Note, too, that the coefficient c_i is fully specified in terms of the relative curvature and material properties at the ith contact. The coefficient β is given by $\beta(e) = \pi\Phi^{1/4}(e)/\sqrt{2}eK^{3/2}(e)$, where $\Phi(e) = (\mathbf{K}(e) - \mathbf{E}(e))((1-e^2)^{-1}\mathbf{E}(e) - \mathbf{K}(e))$.

Several remarks are in order. First, the Hertz formula holds for 3-D bodies. Elasticity theory requires the modeling of 2-D bodies as 3-D cylinders with a cross section identical to the 2-D bodies. Line contact holds between the cylindrical bodies, and this case is summarized in [21]. Second, when the bodies are not quasi-rigid, the Hertzian assumptions are no longer satisfied. It is not adequate to consider only local deformations. Last, it is important to note that the overlap representation (2) is valid under more general circumstances than those assumed by the Hertz model [36]. For example, the surfaces need not be smooth at the contact, and the contact area need not be small compared with the bodies' sizes. So long as the contacts are frictionless and the relative approach of the bodies is reasonably well defined and small, the resultant contact force can be expressed as a function of the overlap.

IV. Computation of the Stiffness Matrix

In this section, we derive a closed-form formula for the stiffness matrix of a grasp in terms of the overlap functions and their derivatives. We begin by expressing the total elastic energy of a k-finger grasp in terms of the overlap functions $\delta_i(q)$. Recall that the magnitude of the ith finger force associated with a given stiffness model is $F_i = f_i(\delta_i)$. The elastic potential energy of a system consisting of a quasi-rigid object $\mathcal{B}$ grasped by quasi-rigid fingers $\mathcal{A}_1, \ldots, \mathcal{A}_k$ is

$$\Pi(q) = \sum_{i=1}^{k} \int_0^{\delta_i(q)} f_i(\sigma) d\sigma. \tag{5}$$

Since f_i is assumed to be differentiable and $\delta_i(q)$ is smooth at points q where $\delta_i(q) > 0$, the elastic energy function Π is differentiable at configurations where all the contacts are loaded.

Suppose that, in the absence of an external wrench, $\mathcal{B}$ is held in equilibrium grasp at a configuration q_0 under the action of *nonzero* preloading forces by each finger. Equilibrium requires that the gradient of Π vanish at q_0. Taking the derivative of Π gives[2]

$$\nabla\Pi(q_0) = \sum_{i=1}^{k} f_i\left(\delta_i(q_0)\right)\nabla\delta_i(q_0) = \vec{0}. \tag{6}$$

Condition (6) is the equilibrium condition (1) expressed in terms of overlap functions.

The stiffness matrix of an equilibrium grasp is defined as the Hessian, $K = D^2\Pi(q_0)$, of the elastic potential energy Π at q_0. Since $\nabla\Pi(q_0) = 0$ at an equilibrium grasp, the behavior of Π in the vicinity of q_0 is determined by K. If K is positive definite, q_0 is a local minimum of Π and the grasp is stable [31]. Thus, we refer to equilibrium grasps with a positive definite stiffness matrix as *stable grasps*. The stiffness matrix also specifies the force-displacement relationship affecting the grasped

[2]We use the differentiation rule $(d/dx)\int_{\phi_1(x)}^{\phi_2(x)} g(\sigma, x)d\sigma = \int_{\phi_1(x)}^{\phi_2(x)} (\partial g/\partial x)d\sigma + g(\phi_2, x)(d\phi_2/dx) - g(\phi_1, x)(d\phi_1/dx)$.

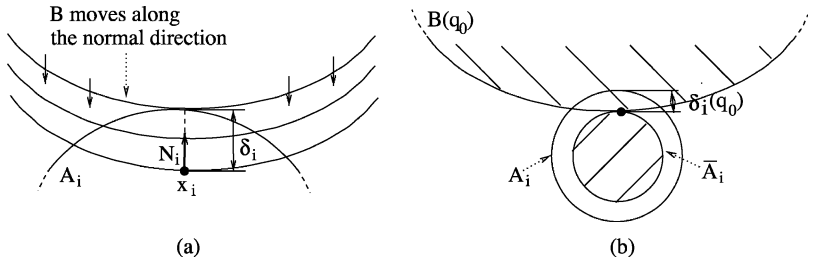

Fig. 4. (a) During normal penetration both x_i and N_i remain unchanged. (b) The imaginary finger $\bar{\mathcal{A}}_i$ obtained by uniformly compressing $\mathcal{A}_i$ by $\delta_i(q_0)$.

object. A small displacement of $\mathcal{B}$ can be approximated by a tangent vector $\dot{q}$, and the fingers react with a wrench which is approximated by $\boldsymbol{w} = K\dot{q}$. To compute the stiffness matrix, we take the derivative of $\nabla\Pi(q)$ and obtain the following key formula.

Theorem 4.1: Let $\mathcal{B}$ be held in a k-finger equilibrium grasp at a configuration q_0, such that the ith finger applies a nonzero force of magnitude $F_i = f_i(\delta_i(q_0))$, where $\delta_i(q_0)$ is the overlap at the ith contact. Then the stiffness matrix of the grasp is

$$K = \underbrace{\sum_{i=1}^{k} f_i'(\delta_i(q_0))\nabla\delta_i(q_0)\nabla\delta_i(q_0)^T}_{K_1} + \underbrace{\sum_{i=1}^{k} f_i(\delta_i(q_0))D^2\delta_i(q_0)}_{K_2} \tag{7}$$

where $f_i' = df_i(\delta_i)/d\delta_i$.

The matrices K_1 and K_2 depend on the initial (or preloading) overlaps $\delta_i(q_0)$. We shall see that both matrices also depend on the contact locations and contact normals. However, K_2 additionally depends on the surface curvature at the contacts. We say that K_1 accounts for first-order geometrical effects, while K_2 accounts for second-order, or surface curvature, effects. The matrix K_1 is always positive semidefinite, since by construction, $f_i'(\delta_i(q_0)) > 0$. If K_1 alone is positive definite, the grasp is said to be *stable to first order*. A first-order stable grasp is stable when, additionally, $K = K_1 + K_2$ is positive definite. If K_1 is positive semidefinite, but the entire matrix K is positive definite, the grasp is said to be *stable to second order*. According to the equilibrium (6), the gradients $\nabla\delta_i(q_0)$ are linearly dependent at q_0. Hence, for K_1 to be positive definite (and the grasp first-order stable), the number of contacts must be at least four in 2-D and at least seven in 3-D. Any stable grasp with a smaller number of contacts must involve curvature effects and be stable to second order. We now turn to the computation of the terms $\delta_i(q_0)$, $\nabla\delta_i(q_0)$, $D^2\delta_i(q_0)$ which appear in (7).

A. Computation of the Overlaps

To compute the overlaps $\delta_i(q_0)$, we first compute the magnitude of the preloading forces, $F_i = f_i(\delta_i(q_0))$ for $i = 1, \ldots, k$. Since each f_i is a known stiffness relationship, the ith overlap is given by $\delta_i(q_0) = f_i^{-1}(F_i)$. We make the following three assumptions. First, we assume that, starting from known initial contact points, the loaded contacts are achieved by pressing the fingers along the contact normals. Since the location of x_i and the direction N_i remain unchanged during this loading process [see Fig. 4(a)], these are known quantities for the loaded grasp. Second, we assume that the sum of the preloading force magnitudes, denoted $f_T = \sum_{i=1}^{k} F_i$ and called the total preloading level, is a known quantity.[3] Third, we restrict our attention to essential equilibrium grasps defined as follows. At an equilibrium grasp, the finger wrenches positively span the origin in wrench space. An essential grasp is defined as a grasp where all fingers must apply a nonzero force in order to positively span the origin. Essential grasps constitute a large class of practical grasps; all generic 2-D grasps with up to four fingers and all generic 3-D grasps with up to seven fingers are essential [30]. In nonessential grasps, the finger-force magnitudes must be determined by direct measurements, rather than by the geometrical procedure described below.

The following lemma, which is proved in Appendix A, asserts that for essential grasps, the finger-force magnitudes are determined up to a common scaling factor by the grasp's first-order geometric properties. By definition, a generating wrench, denoted $\bar{\boldsymbol{w}}_i$, is the wrench generated by a unit force acting along N_i.

Lemma 4.2: Let $\mathcal{B}$ be held in an essential k-finger equilibrium grasp. Then the finger-force magnitudes, $F_i = f_i(\delta_i)$ for $i = 1, \ldots, k$, are determined up to a common scaling factor by the generating wrenches of the grasp, $\bar{\boldsymbol{w}}_1, \ldots, \bar{\boldsymbol{w}}_k$. The common scaling factor mentioned in the lemma is the total preloading level of the grasp, f_T. Once the scaled finger-force magnitudes are computed from the generating wrenches, the actual magnitudes are obtained by multiplying the scaled forces by f_T. The preloading overlaps $\delta_i(q_0)$ are then found by inverting the stiffness functions, $\delta_i(q_0) = f_i^{-1}(F_i)$ $(i = 1, \ldots, k)$.

Example 2: For 2-D or 3-D grasps involving two and three fingers, the normalized finger-force magnitudes can be determined as follows. Let γ_i denote the ith scaled finger-force magnitude. For two fingers, the equilibrium condition $\gamma_1\bar{\boldsymbol{w}}_1 + \gamma_2\bar{\boldsymbol{w}}_2 = 0$ implies that $\gamma_1 = \gamma_2 = 1/2$. For three fingers, the equilibrium condition is $\gamma_1\bar{\boldsymbol{w}}_1 + \gamma_2\bar{\boldsymbol{w}}_2 + \gamma_3\bar{\boldsymbol{w}}_3 = 0$. It can be verified by direct substitution that the solution is $\gamma_i = N_{i+1} \times N_{i+2}$, for $i = 1, 2, 3$, where index addition is performed modulo 3. In this expression, N_i is the inward unit normal at the ith contact, and the cross product for vectors v_1, $v_2 \in \mathbb{R}^2$ is taken as $\det[v_1\ v_2]$.

B. Computation of the Overlap Gradients

The following lemma gives a formula for the overlap gradients.

Lemma 4.3 [31]: Let $\mathcal{B}(q)$ have an overlap of $\delta_i(q) > 0$ with a stationary finger $\mathcal{A}_i$. Let $x_i(q)$ be the endpoint of the overlap

[3] A procedure for determining f_T based on material and geometrical properties of the contacting bodies is described in [21, p. 56–58]. Here we assume that f_T is a given quantity.

segment on the boundary $\mathcal{B}$, and let $N(x_i(q))$ be the inward unit normal to $\mathcal{B}$ at x_i. Then the gradient of δ_i is

$$\nabla\delta_i(q) = \begin{pmatrix} -N\left(x_i(q)\right) \\ \left(Rz_i(q)\right) \times \left(-N\left(x_i(q)\right)\right) \end{pmatrix} \tag{8}$$

where $z_i(q)$ is the point $x_i(q)$ expressed in $\mathcal{B}$'s frame, and R is $\mathcal{B}$'s orientation matrix.

Let us make two clarifying comments. First, $\nabla\delta_i$ is proportional to $-N(x_i)$ in (8), since δ_i increases when $\mathcal{B}$ moves into $\mathcal{A}_i$ along the direction $-N(x_i)$. Second, (8) implies that $-\nabla\delta_i(q)$ is precisely the wrench generated by a unit finger force acting at x_i, while $-f_i(\delta_i)\nabla\delta_i$ is the wrench generated by the ith finger due to an overlap δ_i.

C. Computation of the Overlap Hessians

The last term in the stiffness matrix formula which we need to compute is the Hessian $D^2\delta_i(q_0)$. Let $q(t)$ be a c-space curve such that $q(0) = q_0$ and $\dot{q}(0) = \dot{q}$, where $\dot{q} \in T_{q_0}\mathcal{C}$. To derive a formula for $D^2\delta_i(q_0)$, consider the derivative $(d/dt)|_{t=0}\nabla\delta_i(q(t)) = D^2\delta_i(q_0)\dot{q}$. To simplify the derivation, we decompose the tangent space $T_{q_0}\mathcal{C}$ into the direct sum of two subspaces, $T_{q_0}\mathcal{C} = V_1 \oplus V_2$. The subspace V_1 is the set of $\mathcal{B}$'s instantaneous motions that keep δ_i constant. It is tangent to the level set $S_i = \{q : \delta_i(q) = \delta_i(q_0)\}$ and is given by $V_1 = \{\dot{q} : \nabla\delta_i(q_0) \cdot \dot{q} = 0\}$. The subspace V_2 is tangent to the c-space line, l_i, which passes through q_0 in the direction $(N_i, 0)$. This subspace is given by $V_2 = \{\dot{q} : \dot{q} = \sigma(N_i, 0), \sigma \in \mathbb{R}\}$, and it corresponds to instantaneous pure translations of $\mathcal{B}$ along the normal direction N_i.

A key observation is that $\nabla\delta_i$ remains constant during motion of $\mathcal{B}$ along the c-space line l_i [21], i.e., during pure-translation motion of $\mathcal{B}$ along the normal N_i [Fig. 4(a)]. It follows that $D^2\delta_i(q_0)$ vanishes on the subspace V_2. Hence, we only need to compute $D^2\delta_i(q_0)$ on V_1 and then extend the formula for $D^2\delta_i(q_0)$ from V_1 to the entire tangent space $T_{q_0}\mathcal{C}$.

To compute the derivative of $\nabla\delta_i(q)$ along V_1, let $q(t)$ lie in the level set $\mathcal{S}_i$, such that $q(0) = q_0$ and $\dot{q}(0) = \dot{q} \in V_1$. To evaluate $(d/dt)|_{t=0}\nabla\delta_i(q(t))$, imagine that the physical finger $\mathcal{A}_i$ is replaced with a rigid finger $\bar{\mathcal{A}}_i$, obtained by uniformly compressing $\mathcal{A}_i$ by the amount $\delta_i(q_0)$ [Fig. 4(b)]. Then $\mathcal{B}(q_0)$, which originally overlaps $\mathcal{A}_i$, is in point contact with $\bar{\mathcal{A}}_i$. Furthermore, since $q(t)$ lies in $\mathcal{S}_i$, $\mathcal{B}$ moves along $q(t)$ while maintaining contact with $\bar{\mathcal{A}}_i$. We call such motion a *roll-slide motion* of $\mathcal{B}$ along the surface of $\bar{\mathcal{A}}_i$. Since $\mathcal{S}_i$ is a level set of $\delta_i(q)$, $\nabla\delta_i(q)$ is normal to $\mathcal{S}_i$ at points $q \in \mathcal{S}_i$. Hence, $\dot{q} \cdot (d/dt)\nabla\delta_i(q(t))$ is a scalar multiple of the *curvature* of $\mathcal{S}_i$ along $\dot{q}$. A formula for the curvature of $\mathcal{S}_i$ is known, since $\mathcal{S}_i$ can be interpreted as the boundary of the c-space obstacle corresponding to $\bar{\mathcal{A}}_i$.[4] Using the formula for the curvature of a c-space obstacle [30, p. 707], we obtain that $(d/dt)|_{t=0}\nabla\delta_i(q(t)) = Q_i\dot{q}$, where Q_i is the 6 $\times$ 6 symmetric matrix, given as follows:

$$Q_i = \begin{pmatrix} I & -\hat{p}_i \\ O & \hat{N}_i \end{pmatrix}^T \begin{pmatrix} -L_{\bar{A}_i}\bar{L}_{\rm rel}^{-1}L_{B_i} & L_{\bar{A}_i}\bar{L}_{\rm rel}^{-1} \\ \bar{L}_{\rm rel}^{-1}L_{\bar{A}_i} & \bar{L}_{\rm rel}^{-1} \end{pmatrix} \times \begin{pmatrix} I & -\hat{p}_i \\ O & \hat{N}_i \end{pmatrix} + \begin{pmatrix} O & O \\ O & \left(\hat{N}_i^T\hat{p}_i\right)_s \end{pmatrix}. \tag{9}$$

[4]The c-space obstacle corresponding to $\bar{\mathcal{A}}_i$ is the collection of configurations such that $\mathcal{B}(q)$ intersects $\bar{\mathcal{A}}_i$.

In this formula, O is a 3 $\times$ 3 matrix of zeros, $(A)_S = (1/2)(A^T + A)$, and for a given vector $v \in \mathbb{R}^3$, $\widehat{v}$ is the 3 $\times$ 3 skew-symmetric matrix such that $\widehat{v}u = v \times u$ for all $u \in \mathbb{R}^3$. Moreover, L_{B_i} is the curvature matrix of $\mathcal{B}$ at x_i, $L_{\bar{A}_i}$ is the curvature matrix of $\bar{\mathcal{A}}_i$ at x_i, and $\bar{L}_{\rm rel} = L_{B_i} + L_{\bar{A}_i}$ is the relative curvature matrix of $\mathcal{B}$ and $\bar{\mathcal{A}}_i$ at x_i. Lastly, $p_i = Rz_i$, where z_i is the ith contact point expressed in $\mathcal{B}$'s reference frame and R is the orientation matrix of $\mathcal{B}$.

To extend the formula for $D^2\delta_i(q_0)$ from V_1 to all of $T_{q_0}\mathcal{C}$, we construct in Appendix A a projection matrix P_i. This matrix maps a tangent vector $\dot{q} \in T_{q_0}\mathcal{C}$ to its unique component $\dot{q}_1 \in V_1$, corresponding to the decomposition $T_{q_0}\mathcal{C} = V_1 \oplus V_2$. The following proposition, which is proved in the Appendix, gives the formula for P_i and provides the resulting formula for $D^2\delta_i(q_0)$.

Proposition 4.4: Let $\mathcal{B}(q_0)$ have an overlap of $\delta_i(q_0) > 0$ with a stationary finger $\mathcal{A}_i$. Then the 6 $\times$ 6 Hessian matrix of the overlap function δ_i is

$$D^2\delta_i(q_0) = P_i^T Q_i P_i, \quad \text{where } P_i = \begin{pmatrix} I - N_iN_i^T & N_iN_i^T\hat{p}_i \\ O & I \end{pmatrix} \tag{10}$$

and Q_i is given in (9).

Let us verify that all of the terms in (10) are known. Under a normal loading process [Fig. 4(a)], the quantities N_i and $p_i = Rz_i$ are identical to the respective quantities prior to loading. Similarly, the curvature matrix L_{B_i} is the curvature matrix of $\mathcal{B}$ at the original contact point x_i. As for the curvature matrix $L_{\bar{A}_i}$, it is shown in [21] that $L_{\bar{A}_i} = L_{A_i}(I - \delta_i L_{A_i})^{-1} = (I - \delta_i L_{A_i})^{-1}L_{A_i}$, where L_{A_i} is the curvature matrix of the undeformed finger $\mathcal{A}_i$ at the original contact point. Thus, all of the terms in (10) are computable from the corresponding geometrical quantities prior to the loading process.

Finally, the Hessian formula for planar grasps has the following simpler form. Let r_{B_i} and r_{A_i} denote the radius of curvature of the planar bodies $\mathcal{B}$ and $\mathcal{A}_i$ at their original contact point. The radius of curvature of the imaginary finger $\bar{\mathcal{A}}_i$ is $r_{\bar{\mathcal{A}}_i} = r_{A_i} - \delta_i(q_0)$. *Proposition 4.4* simplifies to the following corollary, for which a proof is sketched.

Corollary 4.5: For a planar grasp, the 3 $\times$ 3 Hessian matrix of the overlap function δ_i is

$$D^2\delta_i(q_0) = \frac{1}{r_{\bar{A}_i} + r_{B_i}} \times \begin{pmatrix} N_iN_i^T - I & (r_{B_i} - \rho_i)JN_i \\ (r_{B_i} - \rho_i)\left(JN_i\right)^T & \left(r_{\bar{A}_i} + \rho_i\right)\left(r_{B_i} - \rho_i\right) \end{pmatrix} \tag{11}$$

where $r_{\bar{A}_i} = r_{A_i} - \delta_i(q_0)$, $\rho_i = -(Rz_i) \cdot N_i$, and

$$J = \begin{pmatrix} 0 & 1 \\ -1 & 0 \end{pmatrix}.$$

Proof Sketch: Let us focus on a single contact and drop the subscript i. The matrix representation of $D^2\delta(q_0)$ is given by that of the quadratic form $F(\dot{q}) = \dot{q}^T D^2\delta(q_0)\dot{q} = \dot{q}^T(P^TQP)\dot{q}^T$, where $\dot{q} = (v_{3\times1}, \omega_{3\times1})$. In the planar case $v_{3\times1} = (v_x, v_y, 0)$, $\omega_{3\times1} = (0, 0, w_z)$, $N_{3\times1} = (N_x, N_y, 0)$, and $p_{3\times1} = (p_x, p_y, 0)$. For notational brevity, we write $v = (v_x, v_y)$, $\omega = \omega_z$, $N = (N_x, N_y)$, and $p = (p_x, p_y)$. Note

that $p = Rz$, where $z = (z_x, z_y)$ and R a planar 2×2 rotation matrix. Using this notation, we obtain

$$\begin{pmatrix} I_{3\times3} & -(\hat{p})_{3\times3} \\ O_{3\times3} & (\hat{N})_{3\times3} \end{pmatrix} P \begin{pmatrix} v_{3\times1} \\ \omega_{3\times1} \end{pmatrix} = \begin{pmatrix} \begin{pmatrix} a \\ 0 \end{pmatrix} \\ \begin{pmatrix} b \\ 0 \end{pmatrix} \end{pmatrix}$$

where a and b are planar vectors *tangent* to the boundary of $\mathcal{B}$ at the contact, given by $a = (I - NN^T)(v - Jp\omega)$ and $b = JN\omega$, with

$$J = \begin{pmatrix} 0 & 1 \\ -1 & 0 \end{pmatrix}.$$

Next, we may think of the planar object $\mathcal{B}$ and the compressed finger $\bar{\mathcal{A}}_i$ as "slabs" obtained by thickening the planar bodies in a direction orthogonal to the plane, along the z axis. These slabs are flat along the z axis, and their 3×3 curvature matrices are given by

$$L_{\bar{A}} = \begin{pmatrix} (L_{\bar{A}})_{2\times2} & 0_{2\times1} \\ 0_{1\times2} & 0 \end{pmatrix} \text{ and } L_B = \begin{pmatrix} (L_B)_{2\times2} & 0_{2\times1} \\ 0_{1\times2} & 0 \end{pmatrix}$$

where $(L_{\bar{A}})_{2\times2}$ and $(L_B)_{2\times2}$ are the 2×2 curvature matrices of $\bar{\mathcal{A}}_i$ and $\mathcal{B}$ at the contact point. Since a is tangent to the boundary of $\mathcal{B}$, we have

$$L_{\bar{A}} \begin{pmatrix} a \\ 0 \end{pmatrix} = \begin{pmatrix} \frac{1}{r_{\bar{A}}} a \\ 0 \end{pmatrix}$$
$$L_B \begin{pmatrix} a \\ 0 \end{pmatrix} = \begin{pmatrix} \frac{1}{r_B} a \\ 0 \end{pmatrix}$$
$$\text{Ł}_{\text{rel}}^{-1} \begin{pmatrix} a \\ 0 \end{pmatrix} = \begin{pmatrix} \frac{1}{\frac{1}{r_{\bar{A}}} + \frac{1}{r_B}} a \\ 0 \end{pmatrix}.$$

Similar equations hold for b. Using these results and expanding $\omega_{3\times1}^T((\hat{N})_{3\times3}^T(\hat{p})_{3\times3})_s\omega_{3\times1}$ straightforwardly, we can write the quadratic form $F(\dot{q})$ in terms of $(v, \omega) \in \mathbb{R}^3$ as

$$\begin{aligned} F(\dot{q}) &= ((a,0),(b,0)) \begin{pmatrix} -L_{\bar{A}}\bar{L}_{\text{rel}}^{-1}L_B & L_{\bar{A}}\bar{L}_{\text{rel}}^{-1} \\ \bar{L}_{\text{rel}}^{-1}L_{\bar{A}} & \bar{L}_{\text{rel}}^{-1} \end{pmatrix} \begin{pmatrix} \begin{pmatrix} a \\ 0 \end{pmatrix} \\ \begin{pmatrix} b \\ 0 \end{pmatrix} \end{pmatrix} \\ &\quad + \omega_{3\times1}^T \left((\hat{N})_{3\times3}^T (\hat{p})_{3\times3} \right)_s \omega_{3\times1} \\ &= (v^T \quad \omega) \begin{pmatrix} NN^T - I & (r_B - \rho)JN \\ (r_B - \rho)(JN)^T & (r_{\bar{A}} + \rho)(r_B - \rho) \end{pmatrix} \begin{pmatrix} v \\ \omega \end{pmatrix} \end{aligned}$$

which proves the corollary. □

When $D^2\delta_i(q_0)$ is substituted into the stiffness matrix formula (7) using the Hertz model, the resulting stiffness matrix agrees with the one obtained by Howard and Kumar [19] using a different approach. However, in their formula, the terms $L_{\bar{A}_i}$ and $r_{\bar{A}_i}$ appear only as L_{A_i} and r_{A_i}, i.e., they neglect the effect of local deformation at the contacts on the fingers' curvature.

Example 3 (Stiffness Matrix of a Planar Grasp With Point Fingers): Let k point fingers hold a planar object $\mathcal{B}$ in equilibrium. Point fingers are fingers for which r_{A_i} is negligible when compared with r_{B_i}, the radius of curvature of $\mathcal{B}$ at the ith contact, as well as the characteristic length of $\mathcal{B}$. Using (8), $\nabla\delta_i(q_0) = (N_i, \eta_i)$, where $\eta_i = (Rz_i) \times N_i \in \mathbb{R}$. For the practical assumption of small overlaps, (11) can be simplified, and (7) reduces to the 3×3 stiffness matrix as follows:

$$\begin{aligned} K = &\sum_{i=1}^{k} f_i'(\delta_i(q_0)) \begin{pmatrix} N_iN_i^T & \eta_iN_i \\ \eta_iN_i^T & \eta_i^2 \end{pmatrix} \\ &+ \sum_{i=1}^{k} \frac{f_i(\delta_i(q_0))}{r_{B_i}} \begin{pmatrix} N_iN_i^T - I & -\rho_iJN_i \\ -\rho_i(JN_i)^T & \rho_i(r_{B_i} - \rho_i) \end{pmatrix}. \end{aligned} \quad (12)$$

[Since $\sum_{i=1}^k f_i(\delta_i(q_0))N_i = 0$ at an equilibrium, $\sum_{i=1}^k(\kappa_i\delta_i/(r_{\bar{\mathcal{A}}_i} + r_{B_i}))(r_{B_i} - \rho_i)JN_i = -\sum_{i=1}^k(\kappa_i\delta_i/r_{B_i})\rho_iJN_i$ in (11).] In the special case where the fingers are linear springs, $f_i(\delta_i(q_0)) = \kappa_i\delta_i(q_0)$ and $f_i'(\delta_i(q_0)) = \kappa_i$, as discussed in *Example 1*. Substitution of these linear-spring relationships into (12) yields a formula for K that agrees with the formulas derived by Nguyen [25] and Funahashi *et al.* [14] for the same linear-spring system. By a similar substitution process, we can obtain the stiffness matrix derived by Ponce [27] for a grasp of a polyhedral object by linear springs with spherical tips.

To summarize, we obtained closed-form expressions for all the terms appearing in the stiffness matrix formula (7). The resulting formula admits any contact model determined by a particular choice of the stiffness functions $f_i(\delta_i)$. When applied to the realistic Hertz contact model, the formula provides an accurate description of grasp stiffness, in terms of the object's and fingers' geometric and material properties. When applied to the linear-spring model, it agrees with the specialized formulas of Nguyen [25] and Ponce [27].

D. Stiffness Matrix in a Gravitational Field

When an object is fixtured or grasped in a gravitational field, the preloading forces at the contacts must balance the gravitational force acting on $\mathcal{B}$. Moreover, gravity affects the grasp stiffness matrix. In the following, z_{cm} denotes the location of $\mathcal{B}$'s center of mass expressed in $\mathcal{B}$'s body coordinates, and $x_{\text{cm}}(q) = R(\theta)z_{\text{cm}} + d$ denotes the location of $\mathcal{B}$'s center of mass in fixed world coordinates, where $q = (d, \theta)$ is $\mathcal{B}$'s configuration. When $\mathcal{B}$ is at a configuration q, the vector from $\mathcal{B}$'s origin to x_{cm}, denoted p_{cm}, is given by $p_{\text{cm}}(\theta) = R(\theta)z_{\text{cm}}$.

Using this notation, the gravity potential energy of $\mathcal{B}$ is given by $U(q) = mg(\boldsymbol{e} \cdot x_{\text{cm}}(q))$, where m is the mass of $\mathcal{B}$, g the gravity constant, and $\boldsymbol{e} = (0, 0, 1)$ the vertical direction. The following lemma specifies the derivatives of $U(q)$ (the formulas are straightforward).

Lemma 4.6: The gradient of U is given by $\nabla U(q) = mg\begin{pmatrix} \boldsymbol{e} \\ p_{\text{cm}}(\theta) \times \boldsymbol{e} \end{pmatrix}$. The second derivative matrix of U is given by

$$D^2U(q) = mg \begin{pmatrix} O & O \\ O & (\hat{\boldsymbol{e}}\hat{p}_{\text{cm}})_s \end{pmatrix}$$

where O is a 3×3 matrix of zeros, $A_s = (1/2)(A + A^T)$, and $\hat{\boldsymbol{e}}$ and $\hat{p}_{\text{cm}}$ are 3×3 skew-symmetric matrices.

The gravitational wrench ∇U can be viewed as generated by a horizontal flat finger $\mathcal{A}_g$ pressing on $\mathcal{B}$'s center of mass along the direction $-\boldsymbol{e}$. Stretching this analogy a bit further, we define as gravitational overlap the quantity $\delta_g(q) = \boldsymbol{e} \cdot x_{\text{cm}}(q)$, and define as gravitational stiffness the constant $f_g = mg$. Under this interpretation, a k-finger grasp consists of $k - 1$ physical fingers and one "gravitational finger." The equilibrium (6) becomes

$\sum_{i=1}^{k-1} f_i(\delta_i(q_0))\nabla\delta_i(q_0) + f_g\nabla\delta_g(q_0) = \vec{0}$. Thus, if there are up to six physical fingers (assuming a 3-D grasp), the sum of the finger-force magnitudes, $f_T = \sum_{i=1}^{k-1} f_i(\delta_i(q_0)) + f_g$, is uniquely determined by the object's mass. The influence of f_T on grasp stability and stiffness is discussed in Section VI.

The stiffness matrix under the influence of gravity becomes $K = K_1 + K_2 + D^2U(q_0)$, where K_1 and K_2 are specified in (7) and $D^2U(q_0)$ is given in the lemma. Inspection of $D^2U(q_0)$ reveals that gravity has no effect on the stiffness of a grasp along the translational degrees of freedom of $\mathcal{B}$. Moreover, only rotations of $\mathcal{B}$ about axes orthogonal to the vertical direction $\boldsymbol{e}$ are affected by gravity. We can interpret the contribution of gravity to the grasp stiffness matrix as coming from a horizontal flat finger $\mathcal{A}_g$ contacting a point-size pin, $\mathcal{B}_g$, attached to $\mathcal{B}$'s center of mass. In that case, $L_{A_g} = O$, while $L_{B_g} = \infty I$. Substitution of these curvature matrices in (9) gives the formula $D^2U(q_0) = f_g D^2\delta_g$. Having seen that gravity can be interpreted as a special finger contacting a point on $\mathcal{B}$, we return to the main course of the paper, which is analysis of the stiffness matrix formula (7).

V. Influence of Curvature on Grasp Stability

The stiffness matrix takes the form $K = K_1 + K_2$ (7). The matrix K_1 depends only on first-order geometrical quantities, location of the contacts and direction of the contact normals, while K_2 also depends on the contact curvatures. For a small number of fingers ($k \leqslant 3$ for 2-D and $k \leqslant 6$ for 3-D), the matrix K_1 is only positive semidefinite. Since K must be positive definite for stability, stable grasps that use a small number of fingers must exploit curvature effects. In this section, we use the stiffness matrix formula to study two fundamental questions. First, under what conditions do curvature effects give rise to contact forces comparable to those generated by first-order geometrical effects? Second, under what conditions are curvature effects are stabilizing? After a preliminary scaling of the stiffness matrix, we analyze the contribution of curvature effects to grasp stability. Then we provide examples that highlight important implications of the analysis.

A. Stiffness Matrix Scaling

To determine when K_2 is comparable with K_1, it is convenient to first scale the stiffness matrix into a dimensionless matrix denoted $\tilde{K}$. We use for this purpose the spectral matrix norm of matrices, defined by $\|P\| = (\lambda_{\max}(P^TP))^{1/2}$, where $\lambda_{\max}(P^TP)$ is the largest eigenvalue of P^TP. We construct a scaling matrix S, such that the matrix $\tilde{K} = S^TKS = S^TK_1S + S^TK_2S$ has the property that $\|S^TK_1S\|$ has an order of magnitude of unity. This is done by defining two characteristic parameters. The first parameter, called the characteristic contact stiffness k_c, is a constant of the order of magnitude of the derivatives $f_i'(\delta_i(q_0))$. We also define an auxiliary parameter, called the characteristic preloading overlap δ_c, as the ratio $\delta_c = f_T/k_c$, where $f_T = \sum_{i=1}^{k} f_i(\delta_i(q_0))$ is the total preloading level. Note that δ_c has the same order of magnitude as the preloading overlaps $\delta_i(q_0)$. The second parameter, denoted l_c, is a characteristic length of the object $\mathcal{B}$.

Let the 6×6 scaling matrix be $S = (1/\sqrt{k_c})\mathrm{diag}(I, (1/l_c)I)$. The scaled stiffness matrix is $\tilde{K} = S^TKS = \tilde{K}_1 + \tilde{K}_2$, such that $\tilde{K}_1 = S^TK_1S$ and $\tilde{K}_2 = S^TK_2S$. Let us first verify that $\|\tilde{K}_1\| \cong 1$ as a result of the scaling operation. We can write $\tilde{K}_1$ as

$$\tilde{K}_1 = S^TK_1S = \frac{1}{k_c}\Gamma\Lambda\Gamma^T$$

where $\Gamma = \mathrm{diag}(I, (1/l_c)I)[\nabla\delta_1(q_0)\cdots\nabla\delta_k(q_0)]$ and $\Lambda = \mathrm{diag}(f_1'(\delta_1(q_0)), \ldots, f_k'(\delta_k(q_0)))$. In general, given a positive semidefinite matrix P, its maximal eigenvalue has the same order of magnitude as its trace, $\|P\| \cong \mathrm{tr}(P)$. In our case, $\tilde{K}_1 = (1/k_c)\Gamma\Lambda\Gamma^T$ is positive semidefinite, and $\mathrm{tr}((1/k_c)\Gamma\Lambda\Gamma^T) \cong (1/k_cl_c^2)\sum_{i=1}^{k} f_i'(\delta_i)\|\nabla\delta_i\|^2$. Since $k_c \cong f_i'(\delta_i)$ and $l_c \cong \|\nabla\delta_i\|$, we obtain that $\|\tilde{K}_1\| \cong 1$. It follows that second-order effects are much smaller than first-order effects when the condition $\|\tilde{K}_2\| \ll 1$ holds true. Next we express the scaled matrix $\tilde{K}_2$ in a more convenient form, as follows:

$$\tilde{K}_2 = S^TK_2S = \sum_{i=1}^{k}\gamma_i\Psi_i$$

where the γ_i's are the normalized force magnitudes, $\gamma_i = f_i(\delta_i(q_0))/f_T$. The 6×6 symmetric matrices Ψ_i are given by

$$\begin{aligned}\Psi_i &= \delta_c\mathrm{diag}\left(I, \frac{1}{l_c}I\right) D^2\delta_i(q_0)\mathrm{diag}\left(I, \frac{1}{l_c}I\right)\\ &= \delta_c\begin{pmatrix}\Phi_{11} & \frac{1}{l_c}\Phi_{12}\\ \frac{1}{l_c}\Phi_{12}^T & \frac{1}{l_c^2}\Phi_{22}\end{pmatrix}\end{aligned} \tag{13}$$

where Φ_{11}, Φ_{12}, and Φ_{22} are the block entries of $D^2\delta_i(q_0)$ specified in (10). In the following, we write $P > 0$ when P is positive definite, and $P \geqslant 0$ when P is positive semidefinite.

B. Influence of Curvature Effects on Grasp Stability

The positive definiteness of the stiffness matrix K implies grasp stability. Since $\tilde{K} = S^TKS$ where S is nonsingular, the positive definiteness of $\tilde{K}$ also implies grasp stability. The scaled stiffness matrix is $\tilde{K} = \tilde{K}_1 + \tilde{K}_2$, and we first consider the influence of $\tilde{K}_1$ on grasp stability. The matrix $\tilde{K}_1$ is given by $\tilde{K}_1 = (1/k_c)\Gamma\Lambda\Gamma^T$, where $\Lambda = \mathrm{diag}(f_1'(\delta_1(q_0)), \ldots, f_k'(\delta_k(q_0)))$. Since $f_i'(\delta_i(q_0)) > 0$, Λ is positive definite, and consequently, $\tilde{K}_1$ is positive semidefinite. Thus, first-order geometrical effects always have a stabilizing influence. However, Γ contains the matrix $[\nabla\delta_1(q_0)\cdots\nabla\delta_k(q_0)]$, whose columns are linearly dependent at an equilibrium grasp. The rank of $\tilde{K}_1$ is, therefore, at most $k-1$. Hence, stable grasps that use a small number of fingers ($k < 4$ in 2-D and $k < 7$ in 3-D) must additionally satisfy $\tilde{K}_2 > 0$ along the kernel of $\tilde{K}_1$.

Next we investigate the influence of $\tilde{K}_2 = \sum_{i=1}^{k}\gamma_i\Psi_i$ on grasp stability. Let us focus on the matrix Ψ_i associated with the ith contact. The matrix Ψ_i can be decomposed into the sum $\Psi_i = \Psi_{a_i} + \Psi_{b_i}$, such that $\Psi_{a_i} \geqslant 0$, while Ψ_{b_i} is indefinite but very small. The decomposition is given in the following lemma, which is proved in [21].

Lemma 5.1: Let $\mathcal{L}_{\bar{A}} = (I - N_i N_i^T) L_{\bar{A}} (I - N_i N_i^T)$, $\mathcal{L}_B = (I - N_i N_i^T) L_B (I - N_i N_i^T)$, and $\mathcal{L}_S = L_{B_i} \widehat{p}_i + \hat{N}_i$. Then the matrix Ψ_i given in (13) can be decomposed as

$$\begin{aligned}\Psi_i &= \Psi_{a_i} + \Psi_{b_i} \\ &= \begin{pmatrix} \delta_c \mathcal{L}_{\bar{A}}^T \bar{L}_{\text{rel}}^{-1} \mathcal{L}_{\bar{A}} & \frac{\delta_c}{l_c} \mathcal{L}_{\bar{A}} \bar{L}_{\text{rel}}^{-1} \mathcal{L}_S \\ \frac{\delta_c}{l_c} \mathcal{L}_S^T \bar{L}_{\text{rel}}^{-1} \mathcal{L}_{\bar{A}} & \frac{\delta_c}{l_c^2} \mathcal{L}_S^T \bar{L}_{\text{rel}}^{-1} \mathcal{L}_S \end{pmatrix} \\ &\quad + \begin{pmatrix} -\delta_c \mathcal{L}_{\bar{A}} & O \\ O & \frac{\delta_c}{l_c^2} \left(-\widehat{p}_i^T \mathcal{L}_B \widehat{p}_i + (\hat{N}_i \widehat{p}_i)_s \right) \end{pmatrix}. \quad (14)\end{aligned}$$

In this decomposition, Ψ_{a_i} is positive semidefinite, and, provided that $\|L_{A_i}\| \ll (1/\delta_c)$ and $\|L_{B_i}\| \ll (1/\delta_c)$, the following holds: $\|\Psi_{b_i}\| = \mathcal{O}(\max\{\delta_c \|L_{A_i}\|, \delta_c \|L_{B_i}\|, (\delta_c / l_c)\})$.

Note that the inequalities $\|L_{A_i}\| \ll 1/\delta_c$ and $\|L_{B_i}\| \ll 1/\delta_c$ usually hold true, since they mean that the characteristic overlap δ_c is significantly smaller than the bodies' radii of curvature at the contact. The lemma asserts that Ψ_{a_i} is always stabilizing. Hence, any destabilizing curvature effects must come from Ψ_{b_i}. To see the influence of Ψ_{b_i} on grasp stability, first consider grasps which are stable to first order. (Since $\tilde{K}_1 > 0$ for such grasps, the number of contacts must be $k \geqslant 4$ in 2-D and $k \geqslant 7$ in 3-D.) The possibly destabilizing effects of Ψ_{b_i} are usually too small to destabilize such grasps, as shown in the following proposition.

Proposition 5.2: Let a grasp be first-order stable (i.e., $\tilde{K}_1 > 0$), such that $\|L_{A_i}\| \ll (1/\delta_c)$ and $\|L_{B_i}\| \ll (1/\delta_c)$ at each of the contacts. Then the grasp is stable (i.e., $\tilde{K} = \tilde{K}_1 + \tilde{K}_2 > 0$) when

$$\begin{aligned}\frac{1}{k_c} \sigma_{\min}^2(\Gamma) \min_{1 \leqslant i \leqslant k} \{ f_i'(\delta_i(q_0)) \} \\ \gg \max_{1 \leqslant i \leqslant k} \left\{ \delta_c \|L_{A_i}\|, \delta_c \|L_{B_i}\|, \frac{\delta_c}{l_c} \right\} \quad (15)\end{aligned}$$

where $\Gamma = \text{diag}(I, (1/l_c) I)[\nabla \delta_1(q_0) \cdots \nabla \delta_k(q_0)]$ and $\sigma_{\min}(\Gamma)$ is the smallest singular value of Γ.

In the proof given in Appendix B, we show that the minimal eigenvalue of $\tilde{K}_1$, denoted $\lambda_{\min}(\tilde{K}_1)$, is bounded from below by the left-hand side (LHS) of (15), while $\|\Psi_{b_i}\|$ is bounded from above by the right-hand side (RHS) of (15). Thus $\lambda_{\min}(\tilde{K}_1) \gg \|\Psi_{b_i}\|$ $(i = 1, \ldots, k)$, and $\tilde{K} > 0$. We note that condition (15) is usually not restrictive, for the following reason. At a first-order stable grasp, the number of contacts is sufficiently large so that the finger wrenches span the entire wrench space at q_0. As long as the finger wrenches do not approximately lie on a lower dimensional subspace of wrench space (making the grasp marginal), $\sigma_{\min}(\Gamma)$ is of the order of unity. Furthermore, in practical grasps, the derivatives $f_i'(\delta_i(q_0))$ have the same order of magnitude, and $\min_{1 \leqslant i \leqslant k} \{ f_i'(\delta_i(q_0)) \}$ is of the order of k_c. The LHS of (15) thus has a unity order of magnitude, while δ_c on the RHS satisfies $\delta_c \ll 1$. Hence, condition (15) usually holds true, and first-order stability usually implies stability. However, when a first-order stable grasp is close to being marginal, condition (15) may be violated. As illustrated in *Example 7* below, such grasps can be actually unstable due to destabilizing curvature effects.

Next, consider the influence of curvature effects in second-order stable grasps. In such grasps, $\tilde{K}_1 \geqslant 0$, and curvature effects supply the stabilizing wrenches along the kernel of $\tilde{K}_1$. The following proposition, which is proved in Appendix B, characterizes the condition under which the wrenches produced by $\tilde{K}_2$ are comparable with the wrenches produced by $\tilde{K}_1$.

Proposition 5.3: Let a grasp be second-order stable (i.e., $\tilde{K}_1 \geqslant 0$ and $\tilde{K} = \tilde{K}_1 + \tilde{K}_2 > 0$). If, at some contact $\|L_{A_i}\| = \mathcal{O}(1/l_c)$, $\|L_{B_i}\| = \mathcal{O}(1/l_c)$, and $\|L_{\text{rel}}\| = \mathcal{O}(\delta_c / l_c^2)$, then generically $\|\Psi_{a_i}\| \cong 1$ and $\|\Psi_{b_i}\| = \mathcal{O}(\delta_c / l_c) \ll 1$. That is, the stabilizing curvature effects are comparable with the stabilizing first-order effects, while the destabilizing effects are small.

The proposition implies that stabilizing second-order effects become more pronounced as $\|L_{\text{rel}}\|$ decreases (as the curvatures of the contacting surfaces achieve a better match). In particular, when the two surfaces fit sufficiently closely, stabilizing second-order effects can become comparable with stabilizing first-order effects. This result has the following practical implication. It has been shown that curvature effects can reduce the number of fixtures needed to immobilize an object [4], [9], [10], [28], [29]. However, it has not been known how much force can be produced by curvature effects, as compared with first-order effects. Our analysis indicates that, by proper choice of the fixels' curvatures, fixtures that exploit curvature effects can be as stiff as fixtures that exploit only first-order effects. Moreover, in many applications, the usually softer curvature effects may be adequate, and close curvature matching would not be necessary.

Significant stabilization via second-order effects can be more easily demonstrated for planar grasps. We introduce the following definition and a planar version of *Proposition 5.3*.

Definition 5.1 (Curvature-Effect Indicator): Let r_{A_i} and r_{B_i} be the radii of curvature of the planar bodies $\mathcal{A}_i$ and $\mathcal{B}$ at their contact point. Let one of the contacting bodies be either concave or flat at the contact. Then the *curvature-effect indicator* at the ith contact is the scalar $\chi = (l_c / r)^2 (\delta_c / \Delta r)$, where $r = \min\{|r_{A_i}|, |r_{B_i}|\}$ and $\Delta r = \| r_{A_i}| - |r_{B_i} \|$.

By definition, χ is proportional to $1/\Delta r$. Hence, higher values of χ indicate a closer curvature match of the contacting bodies.

Corollary 5.4: Let a planar grasp be second-order stable. If, at some contact $(1/r) = \mathcal{O}(1/l_c)$ and $(1/\chi) = \mathcal{O}(1)$, where r and χ are specified in *Definition 5.1*, then generically $\|\Psi_{a_i}\| \cong 1$ and $\|\Psi_{b_i}\| = \mathcal{O}(\delta_c / l_c) \ll 1$. That is, the stabilizing curvature effects are comparable with the stabilizing first-order effects, while the destabilizing second-order effects are small.

The corollary can be interpreted as follows. The condition $(1/r) = \mathcal{O}(1/l_c)$ states that the bodies' radii of curvature must not be too small relative to $\mathcal{B}$'s characteristic dimension l_c. For concreteness, write this condition as $r \geqslant 0.1 l_c$. The condition $(1/\chi) = \mathcal{O}(1)$ can be written for concreteness as $(1/\chi) \leqslant 10$ or, equivalently, $\chi = (l_c / r)^2 (\delta_c / \Delta r) \geqslant 0.1$. Combining the two inequalities, we obtain that if $(\Delta r / r) \leqslant 10^4 (\delta_c / l_c)$ (i.e., if Δr is sufficiently small compared with r), then significant second-order effects can arise. This possibility is discussed in *Examples 5* and *6* below.

C. Examples of Local Curvature Effects

We give four examples that highlight the possible influence of curvature effects on grasp stability. The first two examples show that curvature effects can stabilize a grasp using a small number

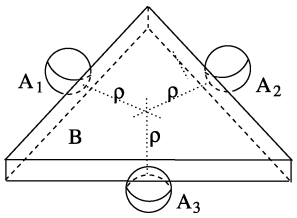

Fig. 5. Grasp of an equilateral triangle by three spherical fingers.

of fingers. In particular, the second example demonstrates that curvature effects can generate stabilizing forces comparable to the forces generated by first-order geometrical effects. The third example further illustrates this possibility by comparing grasps having a different number of fingers. The last example illustrates the impact of destabilizing curvature effects.

Following is a list of assumptions for the examples. First, the fingertips or fixels have an identical spherical shape of radius r_A. Second, the objects are thick slabs undergoing planar motion on a supporting plane. Each object has identical curvatures at the contacts, with a radius of curvature r_B in the horizontal direction, and an infinite radius of curvature in the vertical direction. Third, the Hertz contact model is used to compute the stiffness matrix. Last, the examples consider essential grasps, whose scaled preloading forces are determined as described in Section IV-A. The details behind the examples can be found in [21].

Example 4: This example shows that second-order effects can *stabilize* a grasp which is neutrally stable to first order. Fig. 5 shows an equilateral triangle grasped by three spherical fingers of radius r_A. The origin of $\mathcal{B}$'s frame is chosen at the object's center. We choose the characteristic object length as $l_c = 2\rho$, where $\rho > 0$ is the distance of $\mathcal{B}$'s origin to the contacts. Using *Theorem 4.1* to compute the stiffness matrix $K = K_1 + K_2$, then scaling the stiffness matrix into $\tilde{K} = \tilde{K}_1 + \tilde{K}_2$, we obtain

$$\tilde{K}_1 = \mathrm{diag}(1,1,0) \quad \text{and} \quad \tilde{K}_2 = \mathrm{diag}\left(0,0,\frac{\delta_c(\rho + r_A)}{4\rho^2}\right).$$

The grasp is only neutrally stable to first order with respect to rotations of $\mathcal{B}$ about the origin. However, the grasp is stable after curvature effects are included, since $\tilde{K} = \tilde{K}_1 + \tilde{K}_2$ is positive definite. While the second-order effects are less significant than the first-order effects, they may provide adequate stabilization for many applications, with the added benefit of requiring a smaller number of fingers.

Example 5: This example illustrates how curvature effects can *significantly* stabilize a grasp. Fig. 6(a) shows an object whose boundary consists of three concave circular surfaces of radius $r_B = -3l_c < 0$, where l_c is indicated in the figure. The origin of $\mathcal{B}$'s frame is located at the object's center. The parameter ρ, the distance of $\mathcal{B}$'s origin from the contacts, is given by $\rho = (1/2)(\sqrt{4r_B^2 - 3l_c^2} - 2|r_B| + l_c) = 0.372l_c$. The object is grasped by three fingers with spherical tips of radius $r_A = t|r_B|$, where $0 < t < 1$ is a parameter. Using the Hertz contact model, the scaled stiffness matrix $\tilde{K} = \tilde{K}_1 + \tilde{K}_2$ is found to be

$$\tilde{K}_1 = \mathrm{diag}(1,1,0) \quad \text{and} \quad \tilde{K}_2 = \mathrm{diag}(\xi_T, \xi_T, \xi_R)$$

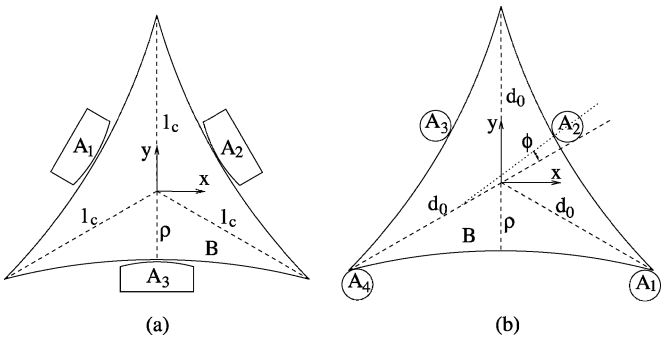

Fig. 6. Top view of a curved triangular object. (a) Grasped by three similarly curved fingers. (b) Grasped by four spherical fingers.

TABLE I
BEHAVIOR OF THREE-FINGER GRASP FOR VARIOUS VALUES OF t

t	χ	ξ_T	ξ_R	a/r_A	a/l_c
0.95	0.122	0.007	0.161	0.049	0.140
0.96	0.164	0.010	0.213	0.053	0.152
0.97	0.237	0.014	0.304	0.058	0.168
0.98	0.393	0.022	0.491	0.066	0.193
0.99	0.899	0.047	1.067	0.081	0.240

where $\xi_T = (2\psi^2/3u)$ and $\xi_R = ((2\xi_T(|r_B| + \rho)(4(|r_B| + \rho) - r_e u))/l_c^2)$, with $u = \psi^2 + ((4(1-t)|r_B|)/r_e)$ and $\psi = (2f_T/\beta(e)E^* r_e^2)^{1/3}$. The terms ξ_T and ξ_R in $\tilde{K}_2$ measure the contribution of curvature effects to the grasp's translational and rotational stiffness. Since the contacting surfaces tend to match perfectly when t approaches unity, we must verify the validity of the Hertz model for these values of t. To do that, it suffices to verify that the major semiaxis of the contact area, a, is small compared with the surfaces' radii of curvature and the object's characteristic dimension. Consider rigid fingers and an aluminum alloy object with $E = 73$ GPa, $\nu = 0.33$, and $E^* = E/(1-\nu^2) = 81.9$ GPa. Then the ratios a/r_A and a/l_c are computed for several values of t in Table I. The small values of these ratios indicate that the Hertz model applies with reasonable accuracy.

Table I also lists the values of the curvature effect indicator χ (Definition 5.1) and the parameters ξ_T and ξ_R. When t approaches unity (the bodies' horizontal curvatures achieve a close match), χ attains an order of unity. By Corollary 5.4, when χ is of the order of unity, second-order stabilizing effects are significant. This is confirmed by the order-of-unity values of ξ_R listed in the table for $t = 0.99$. Thus, as the fingers' curvature approaches the object's curvature, the forces generated by second-order effects become comparable with the forces generated by first-order effects.

Example 6: Fig. 6(b) shows a four-finger grasp of the same triangular object. The fingers have spherical tips of uniform radius $r_A = t|r_B|$ where $0 < t < 1$. Two of the fingers are placed at the endpoints of $\mathcal{B}$'s bottom edge, and two are placed at the side edges, with the normals making an angle $\phi = 4.1°$ with the associated line of symmetry. We wish to compare this grasp with a reference three-finger grasp, chosen to be the one with $t = 0.99$ in *Example 5*. Hence, we choose the same material, preloading level, characteristic contact stiffness, and characteristic overlap. The scaled stiffness matrix $\tilde{K} = \tilde{K}_1 + \tilde{K}_2$

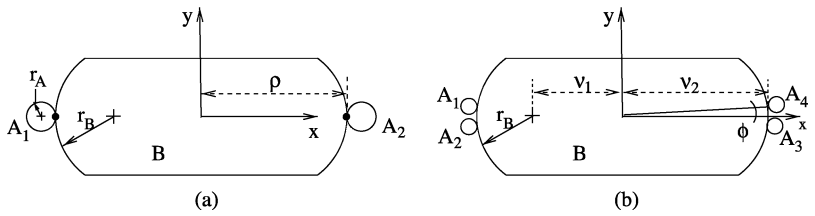

Fig. 7. (a) Top view of an object grasped by two spherical fingers. (b) Same object grasped by four spherical fingers in a way which may become unstable.

TABLE II
BEHAVIOR OF FOUR-FINGER GRASP FOR VARIOUS VALUES OF t

t	χ	$\tilde{K}_1$	$\tilde{K}_2$	$\tilde{K}$
0.5	$7 \cdot 10^{-5}$	$\begin{pmatrix} 0.098 & 0 & 0 \\ 0 & 0.100 & 0 \\ 0 & 0 & 0.088 \end{pmatrix}$	$\begin{pmatrix} 2{\cdot}10^{-5} & 0 & 9{\cdot}10^{-5} \\ 0 & 2{\cdot}10^{-5} & 0 \\ 9{\cdot}10^{-5} & 0 & 2{\cdot}10^{-4} \end{pmatrix}$	$\begin{pmatrix} 0.098 & 0 & 9{\cdot}10^{-5} \\ 0 & 0.100 & 0 \\ 9{\cdot}10^{-5} & 0 & 0.088 \end{pmatrix}$
0.99	0.873	$\begin{pmatrix} 1.164 & 0 & 0 \\ 0 & 1.196 & 0 \\ 0 & 0 & 1.050 \end{pmatrix}$	$\begin{pmatrix} 0.057 & 0 & 0.245 \\ 0 & 0.055 & 0 \\ 0.245 & 0 & 1.215 \end{pmatrix}$	$\begin{pmatrix} 1.221 & 0 & 0.245 \\ 0 & 1.251 & 0 \\ 0.245 & 0 & 2.265 \end{pmatrix}$

is computed for two different values of t and listed in Table II along with the curvature-effect indicator. (The Hertz model can be used with reasonable accuracy, as in *Example 5*.) As predicted by the value of χ, curvature effects enhance grasp stability slightly at $t = 0.5$, and significantly at $t = 0.99$, when the contacting surfaces match closely. Furthermore, at $t = 0.99$, the diagonal entries of $\tilde{K}$ are comparable with those of the three-finger grasp: $\tilde{K} = \mathrm{diag}(1.047, 1.047, 1.067)$. Thus, the three-finger grasp, which relies on curvature effects to achieve stability, has a stability margin comparable with the four-finger grasp, which relies on first-order geometrical effects to achieve stability.

Example 7: The last example shows that second-order effects can *destabilize* a grasp which is stable to first order. Fig. 7(a) shows a symmetric object $\mathcal{B}$ grasped by two spherical fingers of radius r_A. The origin of $\mathcal{B}$ lies at the object's center. The characteristic object length is chosen as $l_c = \rho$, where $\rho > 0$ is the distance from $\mathcal{B}$'s origin to the contacts. Using these parameters, the summands of the scaled stiffness matrix $\tilde{K} = \tilde{K}_1 + \tilde{K}_2$ are $\tilde{K}_1 = \mathrm{diag}(2, 0, 0)$ and $\tilde{K}_2 = -(\delta_c/(r_A + r_B))\mathrm{diag}(0, 1, (\rho + r_A)(\rho - r_B)/\rho^2)$. Hence, $\tilde{K}$ for the two-finger grasp is

$$\tilde{K} = \mathrm{diag}\left(2, -\frac{\delta_c}{r_A + r_B}, -\frac{\delta_c(\rho + r_A)(\rho - r_B)}{\rho^2(r_A + r_B)}\right).$$

Since $\tilde{K}_1 = \mathrm{diag}(2, 0, 0)$, first-order effects are neutral with respect to translations of $\mathcal{B}$ along the y axis and rotations about the origin. Curvature effects, while small, always destabilize the grasp with respect to y translations of $\mathcal{B}$. In contrast, the influence of curvature effects on $\mathcal{B}$'s rotational stability depends on the relative magnitudes of ρ and r_B. The grasp is stable with respect to rotations when $r_B > \rho$ and unstable when $r_B < \rho$.

Fig. 7(b) shows the same object grasped by four spherical fingers. Assuming a positive preload, the grasp is stable to first order. However, the four contacts lie near the contacts of the two-finger grasp of Fig. 7(a). Hence, the four-finger grasp is close to being marginal. The angle ϕ [Fig. 7(b)] indicates how close the four fingers are to the two-finger grasp. It can be shown that the first- and second-order summands of the scaled stiffness matrix are $\tilde{K}_1 = 2\mathrm{diag}(\cos^2\phi, \sin^2\phi, (\nu_1/\nu_2)^2\sin^2\phi)$ and $\tilde{K}_2 = -(f_T/k_c(r_A + r_B))\,\mathrm{diag}(\sin^2\phi, \cos^2\phi, (1/\rho^2)(\rho + r_A)(\rho - r_B))$, where ν_1 and ν_2 are indicated in the figure. Since $\tilde{K}_1$ and $\tilde{K}_2$ vary continuously with ϕ, there is a small neighborhood about $\phi = 0$ in which the destabilizing influence of $\tilde{K}_2$ dominates the stabilizing influence of $\tilde{K}_1$. The grasps corresponding to these values of ϕ are unstable, although they are stable to first order.

VI. INFLUENCE OF PRELOADING ON GRASP STABILITY

In this section, we discuss the combined influence of preloading and geometric effects on grasp stability. We first consider the qualitative influence of preloading on grasp stability, and then discuss the quantitative effect of preloading on the natural compliance of a grasp.

We begin with first-order stable grasps. Recall that such grasps have at least four contacts in 2-D and at least seven contacts in 3-D. *Proposition 5.2* implies that curvature effects are usually negligible in such grasps, and to a good approximation the stiffness matrix consists of the first-order summand K_1 [(7)] as follows:

$$K = K_1 + K_2 \cong \sum_{i=1}^{k} f_i'\left(\delta_i(q_0)\right) \nabla\delta_i(q_0) \nabla\delta_i(q_0)^T.$$

It follows that first-order stable grasps are influenced by the derivative $f_i'(\delta_i(q_0))$ rather than the preloading forces $F_i = f_i(\delta_i(q_0))$. Since $f_i'(\delta_i(q_0)) > 0$ when $\delta_i(q_0)$ is positive, the stability of first-order stable grasps is usually not affected by the specific amount of preloading. However, under realistic contact models, the grasp becomes stiffer for higher preloading forces. This phenomenon has an important practical implication, which is discussed below.

Next, consider first-order stable grasps which are close to being marginal. In such grasps, $K_1 > 0$, but the minimal eigenvalue of K_1 has the same order of magnitude as the maximal eigenvalue of K_2. A precise characterization of such grasps in terms of the geometrical parameters appears in *Proposition 5.2*. Here, let us make two simplifying assumptions: that the overlaps at the contacts have the same order of magnitude and that the stiffness functions at the contacts are uniform. Thus, we write $f_i(\delta_i(q_0)) = f(\delta_c)$ and $f_i'(\delta_i(q_0)) = f'(\delta_c)$, where δ_c is the characteristic overlap at the contacts and f is the uniform stiffness function at the contacts. When we substitute for $f_i(\delta_i(q_0))$ and $f_i'(\delta_i(q_0))$ in (7), the stiffness matrix becomes

$$\begin{aligned} K &= \sum_{i=1}^{k} f_i'\left(\delta_i(q_0)\right) \nabla\delta_i(q_0) \nabla\delta_i(q_0)^T \\ &\quad + \sum_{i=1}^{k} f_i\left(\delta_i(q_0)\right) D^2\delta_i(q_0) \\ &= f'(\delta_c)C_1 + f(\delta_c)C_2 \end{aligned} \tag{16}$$

where $C_1 = \sum_{i=1}^{k} \nabla\delta_i(q_0)\nabla\delta_i(q_0)^T$ and $C_2 = \sum_{i=1}^{k} D^2\delta_i(q_0)$. Note that C_1 contains first-order geometrical effects, while C_2 contains second-order geometrical effects. In order to make concrete statements on the relative influence of $f(\delta_c)$ and $f'(\delta_c)$, let us assume a power law for the stiffness function, $f(\delta_c) = c(\delta_c)^p$, where $p \geqslant 1$. Such a power low is consistent with the linear-spring model ($p = 1$), the Hertz model ($p = 1.5$), and soft fingertip models [36]. Substituting the power law in (16) gives

$$K = pC_1 + \delta_c C_2$$

where we have omitted the common factor $c(\delta_c)^{p-1}$. Since the overlap δ_c is monotonic in the preloading force $f(\delta_c)$, the effect of preloading is to make the relative influence of curvature on grasp stability more pronounced as the amount of preloading increases. A marginal first-order stable grasp can, therefore, be stable for low preloading values and become unstable for high preloading values due to destabilizing curvature effects. This possibility is illustrated in the following example.

Example 7—Continued: The four-finger grasp shown in Fig. 7(b) is marginal for small values of ϕ. The first-order summand of the scaled stiffness matrix, $\tilde{K}_1 = 2\mathrm{diag}(\cos^2\phi, \sin^2\phi, (\nu_1/\nu_2)^2\sin^2\phi)$, is independent on the grasp's total preloading level f_T. In contrast, the second-order summand, $\tilde{K}_2 = -(f_T/k_c(r_A + r_B))\,\mathrm{diag}(\sin^2\phi, \cos^2\phi, (1/\rho^2)(\rho + r_A)(\rho - r_B))$, is proportional to f_T. Thus, when curvature effects are stabilizing (e.g., with respect to rotations of $\mathcal{B}$ when $r_B > \rho$), stabilization is more pronounced with increased preloading. On the other hand, when curvature effects are destabilizing (e.g., with respect to y translations of $\mathcal{B}$), destabilization is more pronounced with increased preloading. Since $\tilde{K}_1$ is independent of f_T, $\tilde{K} = \tilde{K}_1 + \tilde{K}_2$ is positive definite for small f_T, and becomes indefinite due to destabilizing curvature effects for large f_T. In other words, the grasp is stable for low preloading levels, but becomes unstable for high preloading levels. A similar "coin snapping" phenomenon has been observed in frictional two-finger grasps [6], [24], [25].

Finally, consider the influence of preloading on second-order stable grasps. Such grasps are generic when the number of contacts is below four in 2-D and below seven in 3-D. The first-order summand of the stiffness matrix, while only positive semidefinite, is usually nonmarginal. Moreover, curvature has a stabilizing influence along the kernel of the first-order summand. Inspection of (16) reveals that the stability properties of K_1 and K_2 do not change as the amount of preloading increases. Hence, much like first-order stable grasps, the stability of second-order stable grasps is usually not affected by the specific amount of preloading at the contacts. However, the quantitative response of first- and second-order stable grasps to an external wrench varies significantly with the level of preloading. This influence is demonstrated in the following example.

Example 8 (Computing Object Deflection Under Work Load): Fig. 1 shows a thick square plate of edge length $2a$ grasped by four spherical fingers of radius r_A. By definition, the object's *maximal deflection* is the maximal displacement of any of its points induced by an external load. We compute the maximal deflection due to an external torque τ_{ext} (which may be generated by drilling), applied at the square's center. The geometric parameters of the contacts are $r^1_{\mathrm{rel}_i} = r^2_{\mathrm{rel}_i} = r_A$ for $i = 1, \ldots, 4$, $r_e = r_A$, and $\beta(e) = 1$ [21]. By symmetry, the preloading overlaps, forces, and stiffnesses are identical at the four contacts. These quantities are denoted by $\delta_i(q_0) = \delta_c$, $f_i(\delta_i(q_0)) = f(\delta_c)$, and $f'_i(\delta_i(q_0)) = f'(\delta_c)$. Neglecting second-order effects (this is justified by *Proposition 5.2*), the Hertzian stiffness matrix is given by $K = f'(\delta_c)\mathrm{diag}(2, 2, 4a^2)$ [see (7), (8), and (11)]. The object's c-space displacement due to τ_{ext} is given by $\dot{q} = K^{-1}\boldsymbol{w}_{\mathrm{ext}}$, where $\boldsymbol{w}_{ext} = (0, 0, \tau_{\mathrm{ext}})$. Using this $\dot{q}$, the object's maximal deflection occurs at the square's vertices and is given by $\Delta = (\sqrt{2}/4a)(f'(\delta_c))^{-1}\tau_{\mathrm{ext}}$ [21]. For the Hertz contact model, $f'(\delta_c) = (3/2)c\delta_c^{1/2}$, where c is a function of the material and geometrical properties at the contacts. Substituting for f' in Δ gives

$$\Delta = \frac{\sqrt{2}}{6ac}(\delta_c)^{-\frac{1}{2}}\tau_{\mathrm{ext}}.$$

We see that the maximal deflection predicted by the Hertz model decreases with the preloading overlap δ_c. Since $F_i = c\delta_c^{3/2}$ in the Hertz model, the maximal deflection can be written as $\Delta = c_1 F_i^{-1/3}\tau_{\mathrm{ext}}$, where c_1 is a function of the constants a and c. Thus, under the Hertz model, the grasp becomes stiffer as the magnitude of the preloading forces increases.

For comparison, we also compute the object's maximal deflection using a linear-spring contact model. The linear-spring stiffness matrix is given by $K = \kappa\mathrm{diag}(2, 2, 4a^2)$, where κ is the springs' stiffness coefficient. The maximal deflection predicted by the linear-spring model is then

$$\Delta' = \frac{\sqrt{2}}{4a\kappa}\tau_{\mathrm{ext}}.$$

In contrast with the Hertz model, the linear-spring deflection does not depend on the preloading forces (if second-order effects are negligible, as assumed here), and its predictions may therefore deviate significantly from the Hertzian predictions.

VII. Implications of Contact Modeling on Stability

The last example demonstrates that the quantitative assessment of the response of a grasp to an external load significantly depends on the chosen contact model. In this section, we address the corresponding qualitative question. Does the assessment of grasp stability depend upon the chosen contact model, $F_i = f_i(\delta_i)$? We show that, while grasp stability is usually invariant under change of contact model, it is, in general, model dependent. Examples concretely illustrate this fact.

We begin with first-order stable grasps. Recall that $\tilde{K}_1 = (1/k_c)\Gamma\Lambda\Gamma^T > 0$ in such grasps, where $\Lambda = \mathrm{diag}(f'_1(\delta_1(q_0)), \ldots, f'_k(\delta_k(q_0)))$ and $\Gamma = \mathrm{diag}(I, (1/l_c)I)$ $[\nabla\delta_1(q_0)\cdots\nabla\delta_k(q_0)]$. Note that the matrix Γ does not depend on the contact model. Moreover, by construction, $f'_i(q_0) > 0$ when $\delta_i(q_0)$ is positive. Hence, Λ is always positive definite for preloaded grasps. We therefore conclude that first-order stability is model independent. By *Proposition 5.2*, if condition (15) is satisfied, then $\tilde{K} = \tilde{K}_1 + \tilde{K}_2 > 0$ and the grasp is stable. This leads to the following corollary.

Corollary 7.1: Suppose that a grasp is first-order stable (which is a model-independent notion), such that $\|L_{A_i}\| \ll (1/\delta_c)$ and $\|L_{B_i}\| \ll (1/\delta_c)$ at each of the contacts.

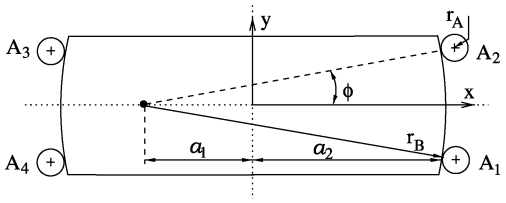

Fig. 8. Top view of an object grasped by four spherical fingers.

Then the grasp is stable under any contact model $F_i = f_i(\delta_i)$ that satisfies the following condition:

$$\frac{1}{k}\sigma_{\min}^2(\Gamma)\min_{1\leqslant i\leqslant k}\{f_i'(\delta_i(q_0))\} \gg \max_{1\leqslant i\leqslant k}\left\{\delta_c\|L_{A_i}\|, \delta_c\|L_{B_i}\|, \frac{\delta_c}{l_c}\right\} \quad (17)$$

where $\sigma_{\min}(\Gamma)$ is the smallest singular value of $\Gamma = \operatorname{diag}(I,(1/l_c)I)[\nabla\delta_1\cdots\nabla\delta_k]$.

The LHS of (17) is usually on the order of unity [21]. On the RHS of (17), usually $\delta_c\|L_{A_i}\| \ll 1$ and $\delta_c\|L_{B_i}\| \ll 1$, as discussed above. Similarly, δ_c on the RHS satisfies $\delta_c \ll l_c$. Thus, the stability of first-order stable grasps is usually model independent. However, the following example shows that when condition (17) is violated, the stability assessment of a first-order stable grasp can become model dependent.

Example 9: Fig. 8 shows an object grasped by four spherical fingers of radius r_A, with the object's radius of curvature at the contacts being r_B. As depicted in the figure, the fingers' locations are determined by the parameters a_1, a_2, and ϕ. By symmetry, the four fingers penetrate the object by the same amount $\delta(q_0)$. A tedious calculation shows that for ϕ small, condition (17) takes the form

$$\sin^2\phi \gg m\frac{\delta(q_0)}{r_A} \quad \text{where} \quad m = \begin{cases} 1, & \text{for the linear-spring model} \\ \frac{2}{3}, & \text{for the Hertz model.} \end{cases} \quad (18)$$

Intuitively, when (18) is violated, the contact normals are nearly horizontal, and the first-order summand in the stiffness matrix is only marginally positive definite. To verify the model dependency predicted by *Corollary 7.1*, let us inspect the grasp's scaled stiffness matrix, $\tilde{K} = \tilde{K}_1 + \tilde{K}_2$. It can be shown that $\tilde{K}_1 = 2\operatorname{diag}(\cos^2\phi, \sin^2\phi, (a_1^2/a_2^2)\sin^2\phi)$ and $\tilde{K}_2 = -2(m\delta(q_0)/(r_A + r_B))\ \operatorname{diag}(\sin^2\phi, \cos^2\phi, ((\rho - r_B)/(r_A + r_B)\rho^2))$, where ρ is the projected length of each contact's position vector onto the associated normal line (Fig. 8). Note that second-order effects are destabilizing along y translations for small ϕ. As ϕ increases, the stabilizing first-order effects become dominant, stabilizing the grasp under both contact models. However, the parameter m has a different value for the Hertz and linear-spring models. Consequently, there is an interval of ϕ values where the grasp is deemed *stable* under the Hertz model while *unstable* under the linear-spring model.

Next, we study the contact model dependency of second-order stable grasps, for which $\tilde{K}_1 \geqslant 0$ while $\tilde{K} = \tilde{K}_1 + \tilde{K}_2 > 0$. The second-order term in the scaled stiffness matrix is given by $\tilde{K}_2 = \sum_{i=1}^k \gamma_i\Psi_i$, where each Ψ_i is given by (13) and can be decomposed according to *Lemma 5.1*. We focus on second-order essential grasps where the normalized finger-force magnitudes γ_i are *model independent* (*Corollary 4.2*). Since the coefficients γ_i in the expression for $\tilde{K}_2$ are model independent, the dependency of $\tilde{K}_2$ on the contact model is caused by the model dependency of $L_{\bar{A}_i}$ and $\bar{L}_{\text{rel}_i} = L_{\bar{A}_i} + L_{B_i}$. $L_{\bar{A}_i}$ depends on the preloading overlap $\delta_i(q_0)$, which is generally model dependent. The following proposition, which is proved in Appendix C, gives a condition under which the assessment of stability for second-order stable grasps remains the same under a change of contact model.

Proposition 7.2: Consider an essential grasp in which $\|L_{A_i}\| = \mathcal{O}(1/l_c)$, $\|L_{B_i}\| = \mathcal{O}(1/l_c)$, and $\|L_{\text{rel}_i}^{-1}\| = \mathcal{O}(l_c)$ at the contacts. Let $\hat{K}_2^0 = \sum_{i=1}^k \gamma_i\Psi_i|_{\delta_i=0}$ with $\Psi_i|_{\delta_i=0}$ obtained by setting $\delta_i = 0$ in Ψ_i, and let U be a matrix whose columns form an orthonormal basis for the null space of $\Gamma = \operatorname{diag}(I,(1/l_c)I)[\nabla\delta_1\cdots\nabla\delta_k]$. If $\lambda_{\min}(U^T\hat{K}_2^0U) \gg (\delta_c/l_c)^2$, the grasp is second-order stable under any contact model $F_i = f_i(\delta_i)$ that satisfies the inequality

$$\frac{1}{k_c}\sigma_{\min}^2(\Gamma)\min_{1\leqslant i\leqslant k} f_i'(\delta_i(q_0)) \gg \frac{\delta_c}{l_c} \quad (19)$$

where $\sigma_{\min}(\Gamma)$ is the smallest nonzero singular value of Γ.

If the radii of curvature and relative radii of curvature of the bodies at the contacts are not too small, the conditions $\|L_{A_i}\| = \mathcal{O}(1/l_c)$, $\|L_{B_i}\| = \mathcal{O}(1/l_c)$, and $\|L_{\text{rel}_i}^{-1}\| = \mathcal{O}(l_c)$ hold true. In the contact-model-dependent inequality (19), the RHS is very small, while $\min_{1\leqslant i\leqslant k} f_i'(\delta_i(q_0))$ often has the same order of magnitude as k_c. Since $\sigma_{\min}^2(\Gamma) \gg \delta_c/l_c$ for nonmarginal grasps, (19) usually holds true. Thus, stability assessment of second-order stable grasps is usually model independent.

We have shown conditions under which the stability of first- and second-order stable grasps is qualitatively insensitive to the choice of contact model. However, even in these typical cases, it is important to note that the quantitative behavior of such grasps is, in general, quite different under different contact models (see *Example 8*). Moreover, when the conditions in *Corollary 7.1* or *Proposition 7.2* are violated, stability analysis may be model dependent. In this case, contact models that are not well justified are inadequate, even for the purpose of qualitative analysis, and the use of well-justified models becomes critical. An example illustrating a grasp arrangement which is stable under a linear-spring model but unstable under the Hertz model is discussed in [21, p. 78–81].

VIII. Effect of Friction on Natural Compliance

In this section, we briefly discuss the effect of friction on the natural compliance of multiple contact arrangements. While a detailed discussion of frictional compliance is beyond the scope of this paper, we can make several observations on the relevance of frictionless compliance when friction is present at the contacts. First, let us introduce some notation. Given a contact force $\boldsymbol{F}_i$, F_i^t and F_i^n denote the projection of $\boldsymbol{F}_i$ along the tangent and inward-normal directions at the ith contact. Also, μ_i denotes the coefficient of friction at the ith contact. Consider now two quasi-rigid bodies which are first loaded against each other

with a normal force of magnitude F_i^n. When the two bodies are subsequently subjected to a tangential loading force of magnitude F_i^t such that $|F_i^t| \leqslant \mu_i F_i^n$, the two bodies deform in a way that generates relative tangential displacement without causing actual sliding of the two bodies [20, p. 210]. Let δ_i^t denote the relative tangential displacement of the two bodies. In our case, one of the bodies is the object $\mathcal{B}(q)$, while the other is a stationary finger $\mathcal{A}_i$. Hence, δ_i^t is a function of q. The tangential force-displacement relationship has been studied theoretically and measured experimentally in the contact-mechanics literature [20]. This relationship has a dominantly elastic nature and to a good approximation has the form

$$F_i^t = g_i\left(\delta_i^t, F_i^n\right) \quad \text{as long as} \quad F_i^n > 0 \quad \text{and} \quad \left|F_i^t\right| \leqslant \mu_i F_i^n. \tag{20}$$

The function g_i has the following properties. It is differentiable, $g_i(0, F_i^n) = 0$, and for any fixed positive F_i^n it is monotonically increasing in δ_i^t. It should be emphasized that (20) only approximates the true tangential force-displacement relationship, which has an inelastic energy dissipating component.

We wish to compute the stiffness matrix associated with the functions g_i $(i = 1, \ldots, k)$. In order to do that, we make the following two assumptions. First, here too, we assume that the initial preloading is obtained by pressing the fingers along the contact normals. In particular, the initial preload forces have zero tangential components. Second, we assume that the variation of g_i with respect to δ_i^t is significantly higher than the variation with respect to F_i^n. This assumption allows us to treat the normal loading F_i^n as being approximately constant. We are now ready to compute the stiffness matrix associated with tangential compliance. Let $\Pi_t(q)$ denote the elastic energy associated with tangential displacements $\delta_1^t(q), \ldots, \delta_k^t(q)$ at the contacts. Then Π_t is given by

$$\Pi_t(q) = \sum_{i=1}^{k} \int_0^{\delta_i^t(q)} g_i\left(\sigma, F_i^n\right) d\sigma. \tag{21}$$

The gradient of Π_t is

$$\nabla\Pi_t(q) = \sum_{i=1}^{k} g_i\left(\delta_i^t(q), F_i^n\right) \nabla\delta_i^t(q). \tag{22}$$

Finally, the Hessian matrix of Π_t is

$$D^2\Pi_t(q) = \sum_{i=1}^{k} g_i'\left(\delta_i^t(q), F_i^n\right) \nabla\delta_i^t(q)\nabla\delta_i^t(q)^T + \sum_{i=1}^{k} g_i\left(\delta_i^t(q), F_i^n\right) D^2\delta_i^t(q) \tag{23}$$

where $g_i' = (\partial/\partial\delta_i^t) g_i(\delta_i^t, F_i^n)$. Let q_0 be the equilibrium-grasp configuration of $\mathcal{B}$. By assumption, $\delta_i^t(q_0) = 0$ for $i = 1, \ldots, k$. Hence, $g_i(\delta_i^t(q_0), F_i^n) = 0$ in (23). Let $\Pi_n(q)$ denote the elastic energy induced by normal displacements at the contacts, given by (5). Then the total elastic energy of the grasp is $\Pi = \Pi_n + \Pi_t$. The Hessian of Π is $D^2\Pi(q_0) = K + \bar{K}$, where $K = D^2\Pi_n(q_0)$ and $\bar{K} = \sum_{i=1}^{k} g_i'(\delta_i^t, F_i^n)\nabla\delta_i^t(\nabla\delta_i^t)^T$. But $\bar{K}$ is positive semidefinite, since $g_i'(\delta_i^t, F_i^n) > 0$ for $i = 1, \ldots, k$. Hence, we can make the following two observations. First, under the above assumptions, friction always enhances the stability of a frictionless grasp arrangement. In particular, if a grasp is stable under the frictionless-contact assumption (i.e., $K > 0$), it remains stable when friction is present at the contacts (i.e., $K + \bar{K} > 0$). Second, under the frictionless contact assumption, an external wrench acting on $\mathcal{B}$ induces a c-space displacement $\dot{q}_1 = K^{-1}\boldsymbol{w}_{\text{ext}}$. When friction is present at the contacts, the c-space displacement of $\mathcal{B}$ is $\dot{q}_2 = [K + \bar{K}]^{-1}\boldsymbol{w}_{\text{ext}}$. In the common case where the external loads are uniformly distributed over a unit ball in wrench space, the largest c-space displacement is obtained by maximizing $\|\dot{q}_i\|$ over all possible external loads $(i = 1, 2)$. The worst-case frictionless and frictional displacements are related by the inequality

$$\max_{\|w_{\text{ext}}\|=1} \{\|\dot{q}_2\|\} \leqslant \max_{\|w_{\text{ext}}\|=1} \{\|\dot{q}_1\|\}. \tag{24}$$

In words, the worst-case frictionless displacement is a conservative upper bound on the worst-case frictional displacement. In practice, one can either obtain a precise expression for g_i from the contact-mechanics literature [20] or use the conservative approximation given by (24).

IX. Concluding Discussion

The use of linear springs to model the natural compliance of multiple contact arrangements is not backed by experimental data or by elasticity theory. In contrast, the classical Hertz model is theoretically justified and has been experimentally verified. Using an overlap function approach, we developed an expression for the grasp stiffness matrix that admits a general class of compliant contact models, including the linear-spring and Hertz models. In the case of the Hertz model, all the constituent terms in the formula are determined from the grasp preloading level and basic material properties and geometrical quantities. Moreover, the quantitative predictions of object deflection made by the Hertzian stiffness matrix can vary significantly from the predictions made by an *an hoc* linear-spring model. The Hertzian stiffness matrix thus provides an accurate and systematic means for modeling the natural compliance of grasp and fixture arrangements. We believe that these results will enable efficient and more reliable algorithms for automated planning of high-precision fixtures, as well as soft-fingertip grasps.

Furthermore, the stiffness matrix formula highlights in closed form the influence of first- and second-order geometric effects on grasp stiffness and stability. We used the formula to show that curvature effects can be used to stabilize a grasp, sometimes significantly, using a smaller number of contacts than would be otherwise required. This result provides a physical basis for methods that synthesize immobilizing grasps based on curvature effects (e.g., [4], [10], and [28]). We further showed that, when a grasp is stabilized only by first-order geometric effects, any destabilizing curvature effects are usually negligible and do not affect the grasp stability. However, there exist grasps in which the stabilizing first-order effects are comparable in magnitude with the destabilizing curvature effects. The relative influence of first- and second-order effects in such grasps depends on the amount of preloading. For low preloading levels, these grasps are stable, but beyond a certain preloading level, they become unstable. To our knowledge, this is the first time a "coin snapping" phenomenon is reported in the context of

frictionless grasps. Finally, we investigated the effect of compliance model choice on grasp stability, showing that stability is generally model dependent. This model dependency offers an additional evidence that the Hertzian model should be preferred in assessing the natural stiffness and stability of grasp arrangements.

While these results are a step forward toward accurate and efficient modeling of compliant grasps and fixtures, further research is needed. First, the classical Hertz model is accurate for bodies that initially touch at a single point. However, when bodies initially touch along a line, the Hertz model may cause inaccuracy to compliance analysis [21, p. 48–50]. Since line contacts are common in workpiece fixturing, improved methods suitable for such contacts need to be developed. Second, the stiffness matrix formula can also be used to characterize the effect of material stiffness on grasp stability. This kind of analysis can provide useful guidelines for selection of fingertip material suitable for a given class of tasks. Third, the formula omits friction. In many fixturing applications, friction is negligibly small, highly dependent on varying environmental factors, or can be ignored for a conservative analysis [5]. In particular, we have shown that frictionless compliance provides a conservative upper bound on object deflection when friction is present at the contacts. However, since friction is important for many lightly loaded grasps, our model should be extended to such cases. We should, however, distinguish such an extension of our work from the traditional approach that models frictional contacts by tangential linear springs (e.g., [19] and [25]). A linear-spring approach is not theoretically or experimentally supported [20], and the proper computation of friction-induced compliance is currently under investigation.

Finally, we are developing an experimental fixturing system for testing the theoretical predictions made in the paper. A description of the system and preliminary experimental data supporting the results of this paper appear in [2].

APPENDIX A
DETAILS OF STIFFNESS MATRIX COMPUTATION

This Appendix contains proofs of statements made in Section IV. First, we prove *Proposition 4.2*, which computes the scaled finger-force magnitudes of a grasp.

Proof of Proposition 4.2

By definition, k vectors $v_1, \ldots, v_k$ in $\mathbb{R}^n$ $(k \leqslant n+1)$ are affinely independent if, for any vector v_j from the set, the $k-1$ vectors $\{v_i - v_j\}_{i=1,\ldots,k, i\neq j}$ are linearly independent. In our case, the vectors $v_1, \ldots, v_k$ are the generating wrenches $\bar{\boldsymbol{w}}_1, \ldots, \bar{\boldsymbol{w}}_k$ (i.e., the wrenches generated by a unit finger force). It is shown in [31] that the generating wrenches of an essential grasp are affinely independent. Hence, we may use the following standard result from convex analysis. Let $v_1, \ldots, v_k$ be affinely independent vectors, and let $\mathcal{P}$ be the convex hull of these vectors. Then any vector $u \in \mathcal{P}$ can be uniquely written as a convex combination $u = \sum_{i=1}^{k} s_i v_i$, such that $s_i \geqslant 0$ and $\sum_{i=1}^{k} s_i = 1$. The coefficients s_i are called barycentric coordinates. The barycentric coordinates of the zero wrench are precisely the scaled finger-force magnitudes of the grasp. □

Next we prove *Proposition 4.4*, giving a formula for $D^2\delta_i(q_0)$. Let $q(t) = (d(t), \theta(t))$ be a c-space curve such that $q(0) = q_0$ and $\dot{q}(0) = \dot{q}$. For each t, let $x_i(q(t)) \in \partial\mathcal{B}(q(t))$ be $\mathcal{B}$'s endpoint of the overlap segment. Let $z_i(q(t)) \in \partial\mathcal{B}$ be the expression of this point in $\mathcal{B}$'s reference frame, i.e., $x_i(q(t)) = R(\theta(t))z_i(q(t)) + d(t)$. We also use the notation $x_0 = x_i(q_0)$, $z_0 = z_i(q_0)$, $N_0 = N(x_i(q_0))$, and $p_0 = R_0 z_0$, where R_0 is the orientation of $\mathcal{B}$ at q_0.

We decompose the tangent space at q_0 into the direct sum $T_{q_0}\mathcal{C} = V_1 \oplus V_2$. The subspace V_1 is tangent to the level set $S_i = \{q : \delta_i(q) = \delta_i(q_0)\}$ and is given by $V_1 = \{\dot{q} : \nabla\delta_i(q_0) \cdot \dot{q} = 0\}$. The subspace V_2 is tangent to the c-space line that passes through q_0 in the direction $\ell_i = (N_0, 0)$, and is given by $V_2 = \{\dot{q} : \dot{q} = \sigma(N_0, 0), \sigma \in \mathbb{R}\}$. The following lemma asserts that V_1 and V_2 induce a direct-sum decomposition on the tangent space $T_{q_0}\mathcal{C}$.

Lemma A.1: For any $\dot{q} \in T_{q_0}\mathcal{C}$, there exist unique $\dot{q}_1 \in V_1$ and $\dot{q}_2 \in V_2$ such that $\dot{q} = \dot{q}_1 + \dot{q}_2$. These two components are given by $\dot{q}_1 = P_i\dot{q}$ and $\dot{q}_2 = (\nabla\delta_i(q_0) \cdot \dot{q})\ell_i$, such that

$$P_i = I_{6\times 6} - \ell_i \nabla\delta_i(q_0)^T = \begin{pmatrix} I - N_0 N_0^T & N_0 N_0^T \hat{p}_0 \\ O & I \end{pmatrix} \quad (25)$$

where $I_{6\times 6}$ is the 6×6 identity matrix.

Proof: The decomposition is straightforwardly verified. Its uniqueness follows from the fact that $V_1 \cap V_2 = \{0\}$. □

It is important to note that $D^2\delta_i(q_0)$ is a *bilinear* function on $T_{q_0}\mathcal{C}$ and that we are seeking the *matrix representation* of this function with respect to the c-space coordinates. Let us still denote this matrix by $D^2\delta_i(q_0)$ and denote by Q_i the matrix representation of $D^2\delta_i(q_0)$ as restricted to V_1. We can now prove *Proposition 4.4* by considering the object $\mathcal{B}$ in point contact with an imaginary finger $\bar{\mathcal{A}}_i$.

Proof of Proposition 4.4

Let $q(t)$ be a parametrization of the c-space line that passes through q_0 at $t = 0$ in the direction ℓ_i. Thus, $q(0) = q_0$ and $\dot{q}(0) = \ell_i \in V_2$. Clearly, $R(\theta(t))$ $z_i(q(t)) \equiv R_0 z_0$ and $N(x_i(q(t))) \equiv N(x_i(q_0))$ (Fig. 4). Hence, $\nabla\delta_i(q(t)) \equiv \nabla\delta_i(q_0)$ and consequently, $(d/dt)|_{t=0}\nabla\delta_i(q(t)) = 0$. Therefore, if one of two tangent vectors $u, v \in T_{q_0}\mathcal{C}$ lies in V_2, then $u^T D^2\delta_i(q_0)v = 0$. Since the vectors $u, v \in T_{q_0}\mathcal{C}$ can be decomposed using *Lemma A.1*, the bilinearity and symmetry of $D^2\delta_i(q_0)$ imply that

$$u^T D^2\delta_i(q_0)v = u^T P_i^T D^2\delta_i(q_0) P_i v, \quad \text{for all } u,\ v \in T_{q_0}\mathcal{C}.$$

Since $P_i u$, $P_i v \in V_1$, the RHS can be written as $u^T P_i^T Q_i P_i v$, and the result follows. □

Remark: In the derivation of $D^2\delta_i$, we may alternatively consider the actual finger $\mathcal{A}_i$ and an imaginary rigid object $\bar{\mathcal{B}}$, obtained by uniformly compressing $\mathcal{B}$ by the amount $\delta_i(q_0)$. In the planar case, the alternative approach yields a formula for $D^2\delta_i$ that contains the term $r_{B_i} = r_{B_i} - \delta_i(q_0)$, the radius of curvature of the compressed object at the contact, and the term

$\bar{\rho}_i = \rho_i - \delta_i(q_0)$. The formula for $D^2\delta_i$ using the alternative approach is

$$D^2\delta_i(q_0) = \frac{1}{r_{A_i} + r_{\bar{B}_i}} \times \begin{pmatrix} N_i N_i^T - I & \left(r_{\bar{B}_i} - \bar{\rho}_i\right) JN_i \\ \left(r_{\bar{B}_i} - \bar{\rho}_i\right)(JN_i)^T & \left(r_{A_i} + \bar{\rho}_i\right)\left(r_{\bar{B}_i} - \bar{\rho}_i\right) \end{pmatrix}. \tag{26}$$

But $r_{B_i} - \bar{\rho}_i = r_{B_i} - \rho_i$ and $r_{A_i} + \bar{\rho}_i = r_{\bar{A}_i} + \rho_i$. Hence, (26) is identical to (11). Similarly, computation of $D^2\delta_i$ in the 3-D case, using the alternative approach, yields a formula which is identical to (10).

Appendix B
Details of Curvature Effects on Grasp Stability

This Appendix contains details of results from Section V. In the proofs, recall that $\lambda_{\min}(P)$ and $\lambda_{\max}(P)$ are the smallest and largest eigenvalues of a symmetric matrix P.

Proof of Proposition 5.2

We have that $\tilde{K} = \tilde{K}_1 + \tilde{K}_2 = \tilde{K}_1 + \sum_{i=1}^{k} \gamma_i \Psi_i$, such that $\Psi_i = \Psi_{a_i} + \Psi_{b_i}$. Since $0 \leqslant \gamma_i \leqslant 1$ and $\Psi_{a_i} \geqslant 0$, it suffices to show that $\lambda_{\min}(\tilde{K}) \geqslant \lambda_{\min}(\tilde{K}_1) - \sum_{i=1}^{k} \|\Psi_{b_i}\| > 0$. In particular, it suffices to show that $\lambda_{\min}(\tilde{K}_1) \gg \|\Psi_{b_i}\|$ for each Ψ_{b_i}. First, $\tilde{K}_1 = (1/k_c)\Gamma\Lambda\Gamma^T$ and $\Gamma\Lambda\Gamma^T \geqslant \lambda_{\min}(\Lambda)\Gamma\Gamma^T$. Hence

$$\begin{aligned} \lambda_{\min}(\tilde{K}_1) &\geqslant \frac{1}{k_c}\lambda_{\min}(\Gamma\Gamma^T)\lambda_{\min}(\Lambda) \\ &= \frac{1}{k_c}\sigma^2_{\min}(\Gamma) \min_{1 \leqslant i \leqslant k} \left\{ f_i'\left(\delta_i(q_0)\right) \right\}. \end{aligned}$$

Since $\|\Psi_{b_i}\| = \mathcal{O}(\max\{\delta_c \|L_{A_i}\|, \delta_c \|L_{B_i}\|, (\delta_c/l_c)\})$ by *Lemma 5.1*, (15) yields $\lambda_{\min}(\tilde{K}_1) \gg \|\Psi_{b_i}\|$. Thus, $\lambda_{\min}(\tilde{K}) > 0$ and the grasp is stable. □

Proof of Proposition 5.3

The assertion $\|\Psi_{b_i}\| = \mathcal{O}(\delta_c/l_c)$ follows directly from *Lemma 5.1*. Hence, it is only necessary to show that $\|\Psi_{a_i}\| \cong 1$. As can be shown, $\bar{L}_{\text{rel}} = L_{\text{rel}} + \delta_i L_{A_i} L_{\bar{A}_i}$. Thus

$$\begin{aligned} \|\bar{L}_{\text{rel}}\| &\leqslant \|L_{\text{rel}}\| + \delta \|L_{A_i}\| \left\|L_{\bar{A}_i}\right\| \\ &= \mathcal{O}\left(\|L_{\text{rel}}\| + \delta_c \|L_{A_i}\|^2 \right) \\ &= \mathcal{O}\left(\frac{\delta_c}{l_c^2} \right) \end{aligned}$$

where we have used $\|L_{\bar{A}_i}\| \cong \|L_{A_i}\|$, as implied by the fact that $\|L_{A_i}\| = \mathcal{O}(1/l_c)$ and $\delta_c/l_c \ll 1$. This bound on $\|\bar{L}_{\text{rel}}\|$ can be used to show that $\|\Psi_{a_i}\| \cong 1$ in the generic case. To this end, it suffices to consider the norm of the lower right diagonal block of Ψ_{a_i}, since the norm of a matrix is bounded from below by the norm of its diagonal blocks. Let P be a symmetric matrix. Then, given a matrix Q, the matrix $Q^T[P - \lambda_{\min}(P)I]Q$ is positive semidefinite. Hence, $\lambda_{\max}(Q^T P Q) \geqslant \lambda_{\min}(P)\lambda_{\max}(Q^T Q)$. Equivalently, $\|Q^T P Q\| \geqslant \|Q\|/\|P^{-1}\|$, since $\lambda_{\min}(P) = 1/\lambda_{\max}(P^{-1})$. In our case $P = \bar{L}_{\text{rel}}^{-1}$ and $Q = \mathcal{L}_S$. Thus, $\|\mathcal{L}_S^T \bar{L}_{\text{rel}}^{-1} \mathcal{L}_S\| \geqslant \|\mathcal{L}_S\|/\|\bar{L}_{\text{rel}}\|$, which gives for the lower right diagonal block of Ψ_{a_i}

$$\frac{\delta_c}{l_c^2}\left\|\mathcal{L}_S^T \bar{L}_{\text{rel}}^{-1} \mathcal{L}_S\right\| \geqslant \frac{\delta_c}{l_c^2}\frac{\|\mathcal{L}_S\|}{\|\bar{L}_{\text{rel}}\|}.$$

We may write the hypothesis $\|\bar{L}_{\text{rel}}\|/(\delta_c/l_c^2) = \mathcal{O}(1)$ as $\|L_{\text{rel}}\| \cong \epsilon(\delta_c/l_c^2)$ where $\epsilon = \mathcal{O}(1)$. Thus, $(\delta_c/l_c^2)\|\mathcal{L}_S^T \bar{L}_{\text{rel}}^{-1} \mathcal{L}_S\| \geqslant \|\mathcal{L}_S\|/\epsilon \cong 1/\epsilon$, where we have used the fact that generically $\|\mathcal{L}_S\| \cong 1$ [21]. Since $\|\Psi_{a_i}\|$ is bounded from below by the norm of its diagonal blocks, $\|\Psi_{a_i}\|$ is at least of the order of magnitude of unity. □

Appendix C
Details of Stability Implications of the Contact Model

In this Appendix, we prove *Proposition 7.2*, which identifies the second-order stable grasps whose stability prediction is model independent. It will be shown that under the conditions given in the proposition, $\|\tilde{K}_2\| \ll 1$ and $\tilde{K}_2$ as such can be considered as a small perturbation to $\tilde{K}_1$. Thus, the following lemma, whose proof is omitted, will be useful when studying the perturbations to the eigenvalues of $\tilde{K}_1$.

Lemma C.1: Let a real symmetric matrix P be perturbed to $P + \Delta P$, where ΔP is real symmetric with $\|\Delta P\| \ll \|P\|$. Let λ be an eigenvalue of P, and T an orthogonal matrix whose columns span the invariant subspace of P associated with λ. Then, $\lambda + x^T \Delta P x$ is an eigenvalue of $P + \Delta P$, where x is a unit-magnitude eigenvector of P associated with λ.

We also need the following two lemmas from [21]. The first lemma characterizes the eigenvalues of the first-order stiffness matrix $\tilde{K}_1$, which is always positive semidefinite. The second lemma expresses $\tilde{K}_2$, which is model dependent, in terms of perturbations to $\tilde{K}_2^0$, which is model independent.

Lemma C.2: Let $\lambda_j(\tilde{K}_1) > 0$ be a nonzero eigenvalue of $\tilde{K}_1$. Then

$$\lambda_j(\tilde{K}_1) \geqslant \frac{1}{k_c}\sigma^2_{\min}(\Gamma) \min_{1 \leqslant i \leqslant k} f_i'\left(\delta_i(q_0)\right)$$

where $\sigma_{\min}(\Gamma)$ is the smallest nonzero singular value of $\Gamma = \text{diag}(I, (1/l_c)I)[\nabla\delta_1(q_0) \cdots \nabla\delta_k(q_0)]$.

Lemma C.3: Consider an essential grasp in which $\|L_{A_i}\| = \mathcal{O}(1/l_c)$, $\|L_{B_i}\| = \mathcal{O}(1/l_c)$, and $\|L_{\text{rel}_i}^{-1}\| = \mathcal{O}(l_c)$ at the contacts. Then $\tilde{K}_2 = \tilde{K}_2^0 + (\delta_c/l_c)\tilde{K}_2^1$, where $\tilde{K}_2^0 = \sum_{i=1}^{k} \gamma_i \Psi_i|_{\delta_i = 0}$ is model independent, and $\tilde{K}_2^1$ is a matrix such that $\|\tilde{K}_2^1\| = \mathcal{O}(\|\tilde{K}_2^0\|)$.

We can now prove *Proposition 7.2*.

Proof of Proposition 7.2

We prove that all the eigenvalues of $\tilde{K}$ are strictly positive. First, using (13) and the conditions $\|L_{A_i}\| = \mathcal{O}(1/l_c)$, $\|L_{B_i}\| = \mathcal{O}(1/l_c)$, and $\|L_{\text{rel}_i}^{-1}\| = \mathcal{O}(l_c)$, it is straightforward to show that $\|\Psi_i\| = \mathcal{O}(\delta_c/l_c)$. Thus, $\|\tilde{K}_2\| = \mathcal{O}(\delta_c/l_c)$, i.e., the curvature effects are small. Since $\|\tilde{K}_1\| \cong 1$, *Lemma C.1* implies that the eigenvalues of $\tilde{K}$ take the form

$$\lambda(\tilde{K}) = \lambda_j(\tilde{K}_1) + x_j^T \tilde{K}_2 x_j$$

where x_j is a unit-magnitude eigenvector of $\tilde{K}_1$ associated with the eigenvalue $\lambda_j(\tilde{K}_1)$. Suppose that $\lambda_j(\tilde{K}_1) > 0$. Then $\lambda_j(\tilde{K}) \geqslant (1/k_c)\sigma^2_{\min}(\Gamma) \min_{1 \leqslant i \leqslant k} f_i'(\delta_i(q_0))$ by *Lemma*

C.2. Since $\|\tilde{K}_2\| = \mathcal{O}(\delta_c/l_c)$, condition (19) implies that $\lambda_j(\tilde{K}) \gg \|\tilde{K}_2\| \geqslant x_j^T \tilde{K}_2 x_j$. Thus, $\lambda(\tilde{K}) > 0$. It remains to consider the case where $\lambda_j(\tilde{K}_1) = 0$. In this case, x lies in the null space of Γ and can be expressed as $x_j = Uy_j$, where $\|y_j\| = 1$. Hence, $\lambda(\tilde{K}) = y_j^T U^T \tilde{K}_2 U y_j \geqslant \lambda_{\min}(U^T \tilde{K}_2 U)$. From *Lemma C.3*, $\tilde{K}_2 = \tilde{K}_2^0 + (\delta_c/l_c)\tilde{K}_2^1$, which by *Lemma C.1* leads to $\lambda_{\min}(U^T \tilde{K}_2 U) = \lambda_{\min}(U^T \tilde{K}_2^0 U) + (\delta_c/l_c) z^T (U^T \tilde{K}_2^1 U) z$, where z is a unit-magnitude eigenvector of $U^T \tilde{K}_2^0 U$ associated with $\lambda_{\min}(U^T \tilde{K}_2^0 U)$. Since $\|U^T \tilde{K}_2^1 U\| \leqslant \|\tilde{K}_2^1\| = \mathcal{O}(\|\tilde{K}_2^0\|) = \mathcal{O}(\delta_c/l_c)$, we have $(\delta_c/l_c) z^T (U^T \tilde{K}_2^1 U) z \leqslant (\delta_c/l_c)\|U^T \tilde{K}_2^1 U\| = \mathcal{O}((\delta_c/l_c)^2)$. Thus, the condition $\lambda_{\min}(U^T \tilde{K}_2^0 U) \gg (\delta_c/l_c)^2$ specified in the proposition implies that $\lambda(\tilde{K}) \geqslant \lambda_{\min}(U^T \tilde{K}_2 U) > 0$. It follows that all of the eigenvalues of $\tilde{K}$ are strictly positive for the contact model under consideration, and the grasp is stable. □

REFERENCES

[1] A. Bicchi, "On the closure properties of robotic grasping," *Int. J. Robot. Res.*, vol. 14, no. 4, pp. 319–334, Aug. 1995.

[2] J. W. Burdick, Y. Liang, and E. Rimon, "Experiments in fixturing mechanics," in *Proc. IEEE Int. Conf. Robotics and Automation*, 2003, pp. 2579–2585.

[3] P. Campbell, *Basic Fixture Design*. New York: Industrial, 1994.

[4] J.-S. Cheong, K. Goldberg, M. H. Overmars, and A. F. van der Stappen, "Fixturing hinged polygons," in *Proc. IEEE Int. Conf. Robotics and Automation*, 2002, pp. 876–881.

[5] Y.-C. Chou, V. Chandru, and M. M. Barash, "A mathematical approach to automatic configuration of machining fixtures: Analysis and synthesis," *ASME J. Eng. Industry*, vol. 111, pp. 299–306, 1989.

[6] M. R. Cutkosky, *Robotic Grasping and Fine Manipulation*. Norwell, MA: Kluwer, 1985.

[7] M. R. Cutkosky and I. Kao, "Computing and controlling the compliance of a robotic hand," *IEEE Trans. Robot. Automat.*, vol. 5, pp. 151–165, Apr. 1989.

[8] M. R. Cutkosky and P. Wright, "Friction, stability and the design of robotic fingers," *Int. J. Robot. Res.*, vol. 5, no. 4, pp. 20–37, 1986.

[9] J. Czyzowicz, I. Stojmenovic, and J. Urrutia, *Immobilizing a polytope*. New York: Springer-Verlag, 1991, vol. 519, Lecture Notes in Computer Science, pp. 214–227.

[10] ——, "Immobilizing a shape," *Int. J. Computat. Geom. Applicat.*, vol. 9, no. 2, pp. 181–206, 1999.

[11] J. P. Donoghue, W. S. Howard, and V. Kumar, "Stable workpiece fixturing," in *Proc. ASME Design Automation Conf.*, 1994, pp. 475–482.

[12] F. Fen, M. Shoham, and R. Longman, "Lyapunov stability of force-controlled grasps with a multifingered hand," *Int. J. Robot. Res.*, vol. 15, no. 2, pp. 137–154, 1996.

[13] H. Fessler and E. Ollerton, "Contact stresses in toroids under radial loads," *Brit. J. Appl. Phys.*, vol. 8, p. 387, 1957.

[14] Y. Funahashi, T. Yamada, M. Tate, and Y. Suzuki, "Grasp stability analysis considering the curvatures at contact points," in *Proc. IEEE Int. Conf. Robotics and Automation*, 1996, pp. 3040–3046.

[15] L. E. Goodman and L. M. Keer, "The contact stress problem for an elastic sphere indenting an elastic cavity," *Int. J. Sol. Struct.*, vol. 1, no. 4, pp. 407–415, 1965.

[16] H. Hanafusa and H. Asada *et al.*, "Stable prehension by a robot hand with elastic fingers," in *Proc. 7th Int. Symp. Industrial Robots*, M. Brady *et al.*, Eds., 1977, pp. 361–368.

[17] H. Hertz, "On the contact of rigid elastic solids and on hardness," in *Miscellaneous Papers by H. Hertz*. London, U.K.: Jones and Schott/Macmillan, 1896. English translation.

[18] E. G. Hoffman, *Jig and Fixture Design*. Albany, NY: Delmar, 1991.

[19] W. S. Howard and V. Kumar, "On the stability of grasped objects," *IEEE Trans. Robot. Automat.*, vol. 12, pp. 904–917, Dec. 1996.

[20] K. L. Johnson, *Contact Mechanics*. Cambridge, U.K.: Cambridge Univ. Press, 1985.

[21] Q. Lin, "Mechanics and planning of workpiece fixturing and robotic grasping," Ph.D. dissertation, Dept. of Mech. Eng., Cal. Inst. of Technol., Pasadena, CA, May 1998.

[22] Q. Lin, J. W. Burdick, and E. Rimon, "A quality measure for compliant grasps," in *Proc. IEEE Int. Conf. Robotics and Automation*, 1997, pp. 86–92.

[23] B. Mishra, "Workholding," in *Proc. IEEE/RSJ Int. Conf. Intelligent Robots and Systems*, 1991, pp. 53–57.

[24] D. J. Montana, "Contact stability for two-fingered grasps," *IEEE Trans. Robot. Automat.*, vol. 8, pp. 230–421, Aug. 1992.

[25] V.-D. Nguyen, "Constructing stable grasps," *Int. J. Robot. Res.*, vol. 8, no. 1, pp. 26–37, 1989.

[26] T. Patterson and H. Lipkin, "Structure of robot compliance," *ASME J. Mech. Des.*, vol. 115, no. 3, pp. 576–580, 1993.

[27] J. Ponce, "On planning immobilizing fixtures for 3D polyhedral parts," in *Proc. IEEE Int. Conf. Robotics and Automation*, 1996, pp. 509–514.

[28] E. Rimon, "A curvature-based bound on the number of frictionless fingers required to immobilize three-dimensional objects," *IEEE Trans. Robot. Automat.*, vol. 17, pp. 679–697, Oct. 2001.

[29] E. Rimon and J. Burdick, "New bounds on the number of frictionless fingers required to immobilize planar objects," *J. Robot. Syst.*, vol. 12, no. 6, pp. 433–451, 1995.

[30] E. Rimon and J. W. Burdick, "Mobility of bodies in contact—Part I: A second-order mobility index for multiple-finger grasps," *IEEE Trans. Robot. Automat.*, vol. 14, pp. 696–708, Oct. 1998.

[31] ——, "Mobility of bodies in contact—Part II: How forces are generated by curvature effects," *IEEE Trans. Robot. Automat.*, vol. 14, pp. 709–717, Oct. 1998.

[32] J. A. Thorpe, *Elementary Topics in Differential Geometry*. Berlin, Germany: Springer-Verlag, 1979.

[33] M. Y. Wang, "A full-kinematic model of fixtures for precision locating applications," in *Proc. IEEE/RSJ Int. Conf. Intelligent Robots and Systems*, 2001, pp. 1135–1140.

[34] D. E. Whitney, "Quasistatic assembly of compliantly supported rigid parts," *J. Dynam. Syst., Meas., Contr.*, vol. 104, pp. 65–77, 1982.

[35] C.-H. Xiong, Y.-F. Li, H. Ding, and Y.-L. Xiong, "On the dynamic stability of grasping," *Int. J. Robot. Res.*, vol. 18, no. 9, pp. 951–958, 1999.

[36] N. Xydas and I. Kao, "Modeling of contact mechanics and friction-limit surfaces for soft fingers in robotics, with experimental results," *Int. J. Robot. Res.*, vol. 18, no. 8, pp. 941–950, 1999.

Qiao Lin received the Ph.D. degree in mechanical engineering from the California Institute of Technology (Caltech), Pasadena, in 1998. His doctoral research involved automated planning of robotic manipulation, with an emphasis on kinematics and mechanics of compliant grasps and fixtures.

He conducted postdoctoral research in microelectromechanical systems (MEMS) at the Caltech Micromachining Laboratory from 1998 to 2000 and has since been an Assistant Professor with the Department of Mechanical Engineering, Carnegie Mellon University, Pittsburgh, PA. His research interests are in MEMS, including micro/nano-fluidic, thermal, and robotic devices for biomedical applications.

Joel W. Burdick received the B.S. degrees in mechanical engineering and chemistry from Duke University, Chapel Hill, NC, and the M.S. and Ph.D. degrees in mechanical engineering from Stanford University, Stanford, CA.

He joined the Department of Mechanical Engineering, California Institute of Technology, Pasadena, in May 1998, and is currently a Professor of Mechanical Engineering and Bioengineering. His current research interests include robotic locomotion, sensor-based robot motion planning, multifingered robotic grasping, neural prosthetics, and applied linear control theory.

Dr. Burdick has received the National Science Foundation Presidential Young Investigator award, the Office of Naval Research Young Investigator award, and the Feynman Fellowship. He has also received the ASCIT Award for excellence in undergraduate teaching and the GSA Award for excellence in graduate student education.

Elon Rimon received the B.Sc. degree in computer engineering from the Technion, Israel Institute of Technology, Haifa, Israel, in 1985, and the Ph.D. degree in electrical engineering from Yale University, New Haven, CT, in 1990.

He has been with the Department of Mechanical Engineering, the Technion, since 1994, where he is currently an Associate Professor. His research interests include geometric reasoning in robotics, sensor-based motion planning, mobile robot problems, grasping and fixturing, and robotic locomotion.